molecular pharmaceutics

Article

pubs.acs.org/molecularpharmaceutics

Mechanistic Analysis of Cocrystal Dissolution as a Function of pH and Micellar Solubilization

Fengjuan Cao, Gordon L. Amidon, Nair Rodriguez-Hornedo, and Gregory E. Amidon*

College of Pharmacy, University of Michigan, Ann Arbor, Michigan 48109-1065, United States

ABSTRACT: The purpose of this work is to provide a mechanistic understanding of the dissolution behavior of cocrystals under the influence of ionization and micellar solubilization. Mass transport models were developed by applying Fick's law of diffusion to dissolution with simultaneous chemical reactions in the hydrodynamic boundary layer adjacent to the dissolving cocrystal surface to predict the pH at the dissolving solid−liquid interface (i.e., interfacial pH) and the flux of cocrystals. To evaluate the predictive power of these models, dissolution studies of carbamazepine−saccharin (CBZ-SAC) and carbamazepine−salicylic acid (CBZ-SLC) cocrystals were performed at varied pH and surfactant concentrations above the critical stabilization concentration (CSC), where the cocrystals were thermodynamically stable. The findings in this work demonstrate that the pH dependent dissolution behavior of cocrystals with ionizable components is dependent on interfacial pH. This mass transport analysis demonstrates the importance of pH, cocrystal solubility, diffusivity, and micellar solubilization on the dissolution rates of cocrystals.

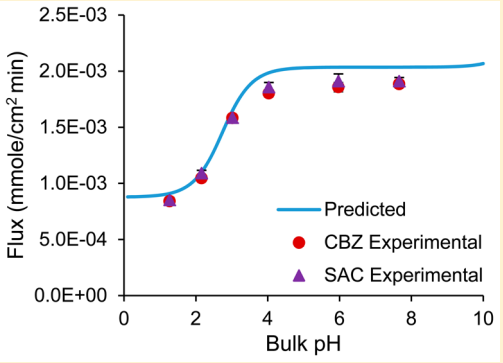

KEYWORDS: *cocrystal dissolution modeling, mass transport analysis, interfacial pH, micellar solubilization, flux predictions, diffusions*

INTRODUCTION

The enhancement of aqueous solubility has remained a challenge for the successful development of new drug products in the pharmaceutical industry as the number of poorly water-soluble drugs is increasing. Many strategies have been employed to overcome this challenge by modifying the solid structure of the drug, and these include amorphous forms, polymorphism, solvates, hydrates, salts, and cocrystals.[1,2] Among these approaches, cocrystalline solids have generated tremendous interest due to their potential advantages over other solid forms, such as their diversity in formation and large solubility range.[2−4] Due to their potential of increasing the bioavailability of drugs, many studies have been carried out to understand the solubility and dissolution behavior of cocrystals.[3,5−9] The solubility behavior of cocrystals has been studied,[10−13] and detailed mechanisms of how solution interactions such as ionization and micellar solubilization affect the solubility of cocrystals have been identified by Rodriguez and co-workers.[14−17] Although there are many dissolution studies of cocrystals in the literature,[3,5−9] only a few have considered the mechanism of dissolution.[12,18,19] A detailed mechanistic understanding of how physicochemical properties of cocrystal components affect the dissolution behavior still remains to be explored. It is essential to understand the dissolution mechanism of cocrystals because such knowledge can provide a better understanding of the oral absorption of drugs from the cocrystalline solids.

An important consideration for cocrystals is the possibility that solution mediated phase transformation (e.g., precipitation of less soluble drug) can occur during dissolution for cocrystals with higher solubility than their parent drugs. This phenomenon has been observed in a number of studies in the literature.[12,19−21] Rapid conversion back to the parent compound makes the measurement of cocrystal dissolution challenging. Dissolution experiments have been carried out at low temperature to decrease the dissolution rates of highly soluble cocrystals to capture the intrinsic dissolution rates; however, phase transformation was still observed.[20] It has also been shown that surfactants can thermodynamically stabilize cocrystals due to differences in micellar solubilization between the drug and coformer.[17,22,23] The critical stabilization concentration (CSC) has been defined as the surfactant concentration required to achieve equivalent solubility of the cocrystal and parent drug.[17] Cocrystals are thermodynamically unstable below the CSC, and crystallization of pure drug can occur, but thermodynamically stable at or above the CSC.[17] Therefore, solid phase transformation can be prevented by performing cocrystal dissolution at or above the CSC.

Cocrystal usually contains a hydrophobic drug and a hydrophilic coformer that have very different physicochemical properties such as ionization, hydrophobicity, and diffusivity. These properties can have very significant effects on the dissolution rates of cocrystals. The ionizable components can undergo simultaneous chemical reactions at the dissolving surface with the chemical species coming from the bulk

Received: November 13, 2015
Revised: January 7, 2016
Accepted: January 15, 2016
Published: February 15, 2016

DOI: 10.1021/acs.molpharmaceut.5b00862
Mol. Pharmaceutics 2016, 13, 1030−1046

solution during dissolution. Consequently, the pH at the dissolving surface is not necessarily equivalent to the bulk solution.[24] The first and most important step for determining the dissolution rate of cocrystal with ionizable components is to model the pH at the dissolving surface. Interfacial pH is affected by the degree of ionization of the component at the interface, which is determined by the concentration and pK_a value of the ionizable component.[24] For single component dissolution, the concentration at the dissolving surface is dictated by the solubility of that component. Diffusivity can also influence the concentrations of the components at the dissolving surface for multicomponent dissolution with different component diffusion coefficients. The faster diffusing component can lead to a decrease in concentration of that component at the dissolving surface.[25] The dissolution of cocrystal is a multicomponent system with different component diffusivities. Therefore, the concentration of the faster diffusing cocrystal component will have a dependence on the difference in diffusivities between the cocrystal components. The larger the difference between the diffusivities, the lower the concentration of the faster diffusing component will be at the surface.

The purpose of this work is to provide a mechanistically realistic physical mass transport analysis of the dissolution behavior of cocrystals under the combined influence of ionization and micellar solubilization. Mass transport models were developed by applying Fick's law of diffusion to dissolution with simultaneous chemical reactions in the hydrodynamic boundary layer adjacent to the dissolving cocrystal surface.[24] To evaluate the predictive power of these models, the constant surface area dissolution rates of two model cocrystals with 1:1 stoichiometric ratio, carbamazepine−saccharin (CBZ-SAC) and carbamazepine−salicylic acid (CBZ-SLC), were determined using a rotating disk dissolution apparatus. Carbamazepine is nonionizable, and saccharin and salicylic acid are monoprotic weak acids with reported pK_a values of 1.6 and 3.0, respectively.[13,17]

MATERIALS AND METHODS

Materials. Anhydrous carbamazepine (CBZ), salicylic acid (SLC), and sodium lauryl sulfate (SLS) were purchased from Sigma Chemical Company (St. Louis, MO) and used as received. Carbamazepine dihydrate (CBZD) was prepared by slurrying anhydrous CBZ in deionized water for 24 h, and solid was obtained through vacuum filtration. Saccharin (SAC) was purchased from Acros Organics (Pittsburgh, PA) and used as received. Isopropanol, acetonitrile, methanol, and hydrochloric acid were purchased from Fisher Scientific (Pittsburgh, PA). Sodium hydroxide pellets were purchased from J.T. Baker (Philipsburg, NJ). Water used in this study was filtered through a double deionized purification system (Milli Q Plus Water System) from Millipore Co. (Bedford, MA).

Cocrystal Synthesis. Cocrystals were prepared by reaction crystallization method[26] at room temperature. CBZ-SAC was prepared by adding 1:1 molar ratio of CBZ and SAC in isopropanol solution. CBZ-SLC was prepared by adding 1:1 molar ratio of CBZ and SLC in acetonitrile solution containing 0.1 M SLC. Solid phases were characterized by X-ray powder diffraction (XRPD) and differential scanning calorimetry (DSC).

Cocrystal Solubility Measurements. Cocrystal solubility was measured by determining the eutectic concentrations of the drug and coformer as a function of SLS concentration at pH 1 and 25 °C. A detailed discussion of the eutectic point measurement was reported elsewhere.[27] Cocrystals (∼100 to 150 mg) and CBZD (∼50 to 100 mg) were suspended in 3 mL of aqueous SLS solution and stirred for 4 days. Samples were collected at 24 h intervals and centrifuged using Corning Costar Spin-X plastic centrifuge tubes with filters to separate the excess solid from solution. Solution concentrations were measured using HPLC, and solid phases were analyzed by XRPD. Cocrystal stoichiometric solubility was determined from the measured eutectic concentrations of the cocrystal components using the method previously developed.[27]

Cocrystal Dissolution Measurements. The constant surface area dissolution rates of cocrystals were determined using a rotating disk apparatus. Cocrystal powder (∼150 mg) was compressed in a stainless steel rotating disk die with a tablet radius of 0.50 cm at approximately 85 MPa for 2 min using a hydraulic press. The die containing the compact was mounted onto a stainless steel shaft attached to an overhead, variable speed motor. The disk was exposed to 150 mL of the dissolution medium in a water jacketed beaker with temperature controlled at 25 °C, and a rotation speed of 200 rpm was used. Dissolution medium was prepared on the day of the experiment by dissolving SLS in water, and solution pH was adjusted using HCl or NaOH. The pH of dissolution media did not change during the experiments at pH 1−3 for both cocrystals. Although the pH decreased for dissolution at pH 4 and above, the final pH was still within the buffering region. This means that the change in bulk pH during dissolution would not have a significant impact on the interfacial pH. Sink conditions were maintained throughout the experiments by ensuring that the concentrations at the last time point of the dissolution were less than 10% of the cocrystal solubility. Solution concentrations were measured using HPLC, and solid phases after dissolution were analyzed by XRPD.

HPLC. Waters HPLC equipped with a photodiode array detector was used for all analysis. The mobile phase was composed of 55% methanol and 45% water with 0.1% trifluoroacetic acid, and the flow rate of 1 mL/min was used. Separation was achieved using a Waters, Atlantis, T3 column (5.0 μm, 100 Å) with dimensions of 4.6 × 250 mm. The sample injection volume was 20 μL. The wavelengths for the analytes were as follows: 284 nm for CBZ, 250 nm for SAC, and 303 nm for SLC.

XRPD. XRPD diffractograms of solid phases were collected with a benchtop Rigaku Miniflex X-ray diffractometer using Cu Kα radiation (λ = 1.54 Å), a tube voltage of 30 kV, and a tube current of 15 mA. Data was collected from 5 to 40° at a continuous scan rate of 2.5°/min.

DSC. Crystalline samples were analyzed by DSC using a TA Instruments 2910 MDSC system equipped with a refrigerated cooling unit. All experiments were performed by heating the samples at a rate of 10 °C/min under a dry nitrogen atmosphere. Temperature and enthalpy of the instrument were calibrated using high purity indium standard.

THEORETICAL

The following mass transport analysis utilizes the classic film theory that postulates the presence of a diffusion boundary layer (i.e., stagnant layer) adjacent to the dissolving surface.[28] The dissolution process is determined by the concentration gradient across the diffusion boundary layer and influenced by the simultaneous diffusion and chemical reactions occurring at the dissolving surface and in the adjacent boundary layer.[24] For

DOI: 10.1021/acs.molpharmaceut.5b00862
Mol. Pharmaceutics 2016, 13, 1030−1046

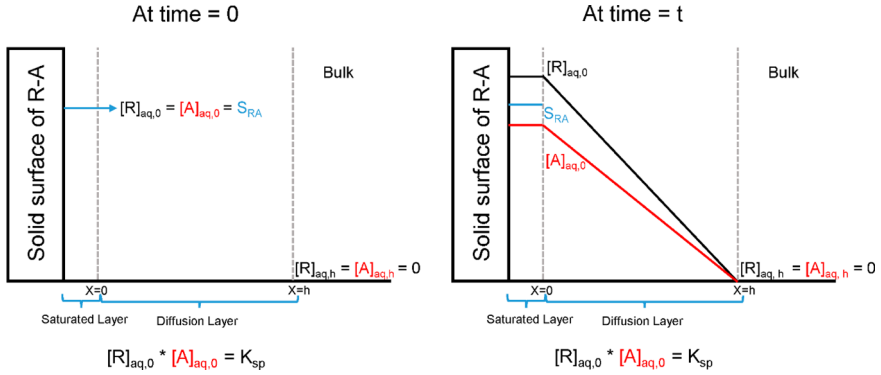

Figure 1. Schematic representation of the dissolution process of RA in nonreactive media using the interfacial equilibrium model. $[R]_{aq,0}$ and $[A]_{aq,0}$ represent the concentrations of R and A at the dissolving surface; $[R]_{aq,h}$ and $[A]_{aq,h}$ represent the concentrations of R and A in the bulk assuming sink conditions; S_{RA} is the solubility of the cocrystal, and K_{sp} is the solubility product of the cocrystal.

the dissolution of a 1:1 cocrystal in nonreactive media (e.g., no ionization or micellar solubilization), the cocrystal would first dissolve according to its solubility product to give equal molar concentrations of the drug and coformer. Both components would then diffuse across the boundary layer into the bulk solution based on their diffusion coefficients and concentration gradients. Cocrystalline solids have well-defined stoichiometry so they will dissolve according to their stoichiometric ratios assuming that there is no precipitation.

At steady state, the dissolution rate of the drug must be the same as that of the coformer for a 1:1 cocrystal if there is no solid phase transformation during dissolution (e.g., drug precipitation). As mentioned above, diffusion across the boundary layer is influenced by component diffusion coefficients, and for most cocrystals, the drug molecule is larger than the coformer, so the diffusion coefficient of the drug is usually less than that of the coformer. The difference in diffusivities between the cocrystal components may be magnified if the dissolution is performed in surfactant solution where the drug may be highly solubilized by micelles, but the coformer is only slightly solubilized. Micellar solubilization typically reduces the diffusion rate of the drug significantly compared to the coformer due to the much lower diffusion coefficient of the drug loaded micelles. With slower diffusion, the transport rate of the drug would be less than that of the coformer. To maintain stoichiometric dissolution of both components of the cocrystal, the difference in diffusivities can influence the concentrations of the components at the dissolving surface under steady state conditions.

The mass transport process of cocrystals may be analyzed in two ways described here as the interfacial equilibrium and the surface saturation models. Both of these models were developed based on the classic film theory of dissolution[28] and the solubility product behavior of cocrystals. The major difference between the two models is related to the boundary conditions at the solid−liquid interface. For the interfacial equilibrium model, the solubility product of the cocrystal is assumed to apply at the dissolving surface at all times $t \geq 0$. For the surface saturation model, the concentration of the slower diffusing component, typically the drug, is maintained equal to the stoichiometric solubility of the cocrystal while the concentration of the faster diffusing component, typically the coformer, is depleted due to its more rapid diffusion. Due to the depletion of the coformer at the dissolving surface, the solubility product of the cocrystal is not maintained for the surface saturation model. It is appropriate to point out that the application of rotating disk hydrodynamics and the associated hydrodynamic boundary layer are simplifying assumptions where simultaneous chemical reactions and micelle solubilization occur. However, useful predictions may be obtained that provide insight into the mechanisms and rate limiting processes impacting dissolution. More detailed descriptions of the two models are provided in the following sections.

Both models are based on the following assumptions: chemical reactions and solute solubilization within the diffusion layer occur instantaneously, free solute and micelle are in equilibrium throughout the diffusion layer, the ionized form of the coformer is not solubilized by surfactant, the solubilization constant of the coformer does not change with surfactant concentration, and aqueous diffusivity of the ionized and nonionized forms are the same. For simplification of the interfacial pH prediction, the effective diffusivity of the coformer is assumed to be the same as the aqueous diffusivity because it is not significantly solubilized by the surfactant. In this study, the effect of surfactant concentration on the viscosity of dissolution media was not accounted for in the mass transport analysis. Although the viscosity of the dissolution media may approximately double at high surfactant concentration (e.g., 300 mM),[29] its impact on the hydrodynamic boundary layer is small as shown in eq 10. The viscosity of dissolution media is not expected to significantly affect the diffusion of free species as they are assumed to be diffusing through the aqueous phase where the surfactant concentration is equal to the critical micellar concentration (CMC) and the viscosity is not substantially different from that of water.[30] The effect of viscosity on the diffusion coefficient of the micelles incorporates the effect of viscosity changes.

Interfacial Equilibrium Model. A schematic representation of the dissolution process for a 1:1 cocrystal with nonionizable components, RA, where R is drug and A is coformer, in nonreactive media, is shown in Figure 1. The first step of dissolution is the formation of a saturated solution at the solid−liquid interface, which represents the equilibrium between the solid cocrystal and solution. This leads to the dissociation of RA into its components, R and A, according to the solubility product, K_{sp}, as described by the following equations:

$$(RA)_s \rightleftharpoons R_{aq} + A_{aq} \quad (1)$$

$$K_{sp} = [R]_{aq}[A]_{aq} \quad (2)$$

DOI: 10.1021/acs.molpharmaceut.5b00862
Mol. Pharmaceutics 2016, 13, 1030−1046

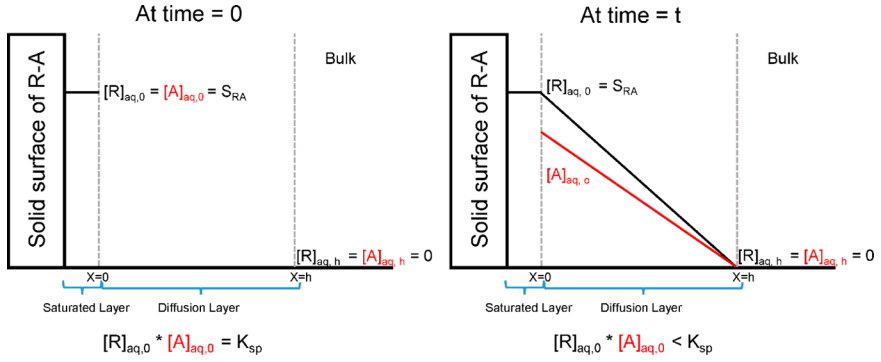

Figure 2. Schematic representation of the dissolution process of RA in nonreactive media using the surface saturation model. $[R]_{aq,0}$ and $[A]_{aq,0}$ represent the concentrations of R and A at the dissolving surface; $[R]_{aq,h}$ and $[A]_{aq,h}$ represent the concentrations of R and A in the bulk assuming sink conditions; S_{RA} is the solubility of the cocrystal; and K_{sp} is the solubility product of the cocrystal.

where subscript s denotes the solid phase and aq denotes the aqueous phase.

At time = 0, before any component diffusion, the concentration of the drug in the saturated layer should be the same as that of the coformer for 1:1 cocrystals as shown in Figure 1. As diffusion occurs, the chemical equilibrium shown in eq 1 is disrupted in the saturated layer because of the decrease in concentration of A due to its more rapid diffusion. To re-establish this equilibrium in the saturated layer, which means keeping K_{sp} constant, the concentrations of R and A would have to vary. A boundary condition assumption at the solid−liquid interface for the interfacial equilibrium model is that the K_{sp} relationship is assumed to apply at all times ($t \geq 0$). Because of the different diffusivities between the cocrystal components, the concentrations of R and A will differ at the dissolving surface for $t > 0$ to maintain stoichiometric dissolution. At steady state, the concentration of R at the solid−liquid interface would be higher than the stoichiometric solubility of the cocrystal due to its lower diffusion coefficient, while the concentration of A is consequently smaller to maintain the K_{sp}.

If there is no solid phase transformation or precipitation in the boundary layer or at the solid surface, the dissolution rate of the drug must be the same as that of the coformer for a 1:1 cocrystal. The dissolution rate of the cocrystal in terms of components can be described by the Nernst−Brunner equation[28,31] for flux:

$$J_R = \frac{D_R[R]_{aq,0}}{h} = J_A = \frac{D_A[A]_{aq,0}}{h} \tag{3}$$

where D is diffusivity, $[R]_{aq,0}$ and $[A]_{aq,0}$ are total concentrations of the drug and coformer at the dissolving surface, h is the thickness of the hydrodynamic boundary layer that reflects the hydrodynamic conditions near the dissolving surface, and sink conditions are assumed. Since this model is assumed to maintain K_{sp}, the following relationship is true at all times:

$$[R]_{aq,0} \times [A]_{aq,0} = K_{sp} \tag{4}$$

The concentration of coformer, $[A]_{aq,0}$, and drug, $[R]_{aq,0}$, at the solid−liquid interface can be solved using eqs 3 and 4 as follows:

$$[A]_{aq,0} = \left(\frac{D_R}{D_A}\right)^{1/2}\sqrt{K_{sp}} \tag{5}$$

$$\begin{aligned}[R]_{aq,0} &= \left(\frac{D_A}{D_R}\right)[A]_{aq,0} \\ &= \left(\frac{D_A}{D_R}\right)\left(\frac{D_R}{D_A}\right)^{1/2}\sqrt{K_{sp}} \\ &= \left(\frac{D_A}{D_R}\right)^{1/2}\sqrt{K_{sp}}\end{aligned} \tag{6}$$

The concentrations of both components at the surface are dependent on the solubility and differential diffusivity between the components. A large difference between the component diffusivities increases the concentration difference between the drug and coformer at the solid−liquid interface while maintaining the solubility product.

Surface Saturation Model. The dissolution process of RA in nonreactive media can also be described using the surface saturation model, illustrated in Figure 2. It is assumed that a saturated layer adjacent to the dissolving surface consists of equal molar concentrations of R and A at the saturated solubility of the cocrystal (i.e., stoichiometric cocrystal solubility) at time = 0. Before any component diffusion, the concentration product of both components within the saturated layer is equal to the solubility product of the cocrystal. Both components then diffuse across the diffusion layer at equal rates in proportion to their respective diffusion coefficients. As diffusion begins, the concentrations of both components would be depleted, but the depletion of A would be greater because of its greater diffusivity compared to R. In response to the depletion, more solid cocrystal would dissolve to maintain a saturated solution corresponding to the solubility of the cocrystal in the saturated layer. R being the slower diffusing component, its rate of depletion determines the rate of replenishment. Therefore, the concentration of R at the dissolving surface is maintained at the stoichiometric solubility of the cocrystal:

$$[R]_{aq,0} = \sqrt{K_{sp}} \tag{7}$$

while the concentration of A may be lower. By assuming that the dissolution rate of the drug is equal to that of the coformer, the concentration of A at the surface can be solved as follows:

$$J_R = \frac{D_R\sqrt{K_{sp}}}{h} = J_A = \frac{D_A[A]_{aq,0}}{h} \tag{8}$$

DOI: 10.1021/acs.molpharmaceut.5b00862
Mol. Pharmaceutics 2016, 13, 1030−1046

$$[A]_{aq,0} = \frac{D_R}{D_A}\sqrt{K_{sp}} \quad (9)$$

The concentration of the drug at the surface is the same as the stoichiometric solubility of the cocrystal, but the coformer concentration is dependent on both the cocrystal solubility and differential diffusivity between the cocrystal components. The greater the difference in diffusivity, the lower the concentration of coformer at the surface. Because of the lower coformer concentration, the solubility product no longer applies beyond the interface at $x > 0$.

The assumptions made for both models are based upon the fact that the diffusion coefficients of the cocrystal components are different. Under stoichiometric dissolution for a 1:1 cocrystal, the dissolution rates of both species are observed to be equal with no solid phase transformation. The difference in diffusion coefficients can result in unequal concentrations of the cocrystal components at the dissolving surface and impact the ability of the cocrystal to maintain the solubility product, K_{sp}. The interfacial equilibrium model is assumed to maintain constant K_{sp} at all times at the dissolving surface during dissolution with the result that the drug concentration is higher but the coformer concentration is lower. The surface saturation model assumes that the drug concentration remains equal to the stoichiometric solubility of the cocrystal, but with a lower coformer concentration to maintain stoichiometric dissolution and without maintaining K_{sp} constant at the dissolving surface. If the drug and coformer have equal diffusion coefficients, the concentrations of both components at the surface will be the same and the two models will merge into one.

Rotating Disk Dissolution Hydrodynamics. Dissolution experiments may be performed using a variety of experimental systems. For this study, rotating disk dissolution experiments were performed. Two significant advantages of this system include the maintenance of a constant surface area available for dissolution as well as defined hydrodynamics that provide an a priori estimate of the hydrodynamic boundary layer adjacent to the rotating surface. According to Levich,[32] the hydrodynamic boundary layer thickness, h, is given by

$$h = 1.612D^{1/3}\nu^{1/6}\omega^{-1/2} \quad (10)$$

where ν is the kinematic viscosity and ω is the angular velocity in radians per unit time.

Both interfacial equilibrium and surface saturation models described above are based on the assumption that the diffusion layer is the same for both the drug and coformer. However, according to eq 10, the diffusion layer thickness has a dependence on the diffusion coefficient. The diffusion coefficients of the drug and coformer in water can be different due to their molecular size difference. The different hydrophobicity between the drug and coformer can also magnify the difference in diffusivity in surfactant solution. The differential diffusivity can result in a significant difference between the diffusion layer of the two cocrystal components as h is directly proportional to the diffusion coefficient.

An alternative approach for the two models is to redefine the diffusion layer thicknesses for both the drug and coformer as they have different diffusion coefficients and consequently different diffusion layer thicknesses according to eq 10. Applying eq 10 separately for the diffusion layer of R ($h_R = 1.612D_R^{1/3}\nu^{1/6}\omega^{-1/2}$) and A ($h_A = 1.612D_A^{1/3}\nu^{1/6}\omega^{-1/2}$) to eq 3 and applying eq 4, the concentrations of R and A at the dissolving surface for the interfacial equilibrium model are shown to become a function of the diffusion coefficients:

$$[A]_{aq,0} = \left(\frac{D_R}{D_A}\right)^{1/3}\sqrt{K_{sp}} \quad (11)$$

$$[R]_{aq,0} = \left(\frac{D_A}{D_R}\right)^{1/3}\sqrt{K_{sp}} \quad (12)$$

And similarly, applying eq 10 separately for R and A to eq 8, the concentration of A at the surface for the surface saturation model becomes

$$[A]_{aq,0} = \left(\frac{D_R}{D_A}\right)^{2/3}\sqrt{K_{sp}} \quad (13)$$

and $[R]_{aq,0}$ is given by eq 7.

Dissolution in Reactive Media. Cocrystals can contain components with different ionization properties (e.g., nonionizable drug and ionizable coformer), and these components can undergo chemical reactions at the solid–liquid interface and in the boundary layer with the species from the bulk solution. These reactions can alter the pH and concentrations at the dissolving surface. A schematic representation of the dissolution process for a 1:1 cocrystal with R as the nonionizable drug and HA as the monoprotic acidic coformer is shown in Figure 3. As cocrystal is initially exposed to solution, it dissociates into its components, R and HA, at the dissolving surface. Both R and HA diffuse across the diffusion layer with a thickness of h, however, HA can simultaneously react with incoming base (B^-) from the bulk solution to form A^- and HB.

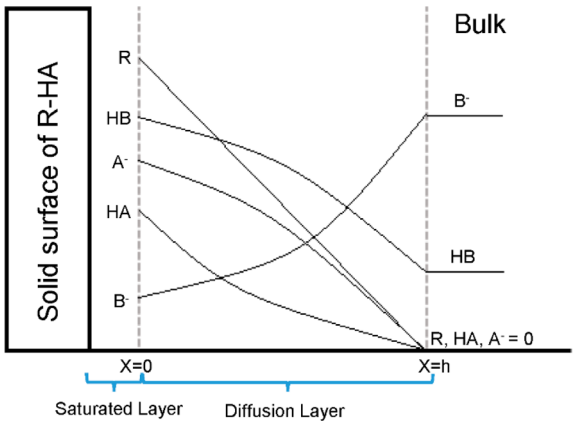

Figure 3. Schematic representation of the dissolution process for a 1:1 cocrystal with R as the nonionizable drug and HA as the monoprotic acidic coformer in the presence of a reactive medium containing base, B^-. A^- and HB are the products of the reaction.

For the dissolution of RHA in a reactive medium containing hydroxide ion and water as the reactive basic species (e.g., no additional buffer), the chemical reactions occurring at the surface and within the boundary layer include the self-dissociation of the cocrystal into R and HA and ionization of HA as it is a weakly acidic coformer. The chemical equilibria and the equations for equilibrium constants for the dissolution of RHA are provided in the Appendix.

Dissolution in Surfactant Solution. Previous studies have shown that surfactants can solubilize the cocrystal components

DOI: 10.1021/acs.molpharmaceut.5b00862
Mol. Pharmaceutics 2016, 13, 1030–1046

to different extents due to the different hydrophobicity of the drug and coformer.[17,22,23] Typically, the drug component is more hydrophobic and it is highly solubilized by surfactants compared to the coformer. The equilibria reflecting the solubilization of drug (R) and the un-ionized form of coformer (HA) are given in the Appendix.

Because of the differential solubilization, the parent drug, which is typically less soluble than the cocrystal in the absence of surfactant, can achieve the same solubility as the cocrystal in solution containing surfactant concentration at the CSC.[17,22,23] As surfactant concentration exceeds the CSC, the parent drug becomes more soluble, so drug precipitation during dissolution of the cocrystal can be prevented. The two cocrystals studied here have higher solubility than the parent drug, so dissolution experiments were performed in media containing surfactant concentrations above the CSC to prevent solid phase transformation. Among the surfactants studied in our lab, sodium lauryl sulfate (SLS) solubilizes CBZ to the greatest extent so it was chosen to study in this work.

Mass Transport Analysis. Detailed derivations of the mass transport analysis for the two models applying the above considerations are provided in the Appendix. The different boundary conditions of the cocrystal components from the two models lead to different mass transport analyses. These mass transport analyses allow for predictions of cocrystal flux as a function of bulk pH and surfactant concentration by taking the pH at the surface into consideration. The comparison of the mass transport analyses between the two models is shown in Results.

RESULTS

Physicochemical Properties. The physicochemical properties of the cocrystal and its components such as solubility products, ionization constants, micellar solubilization constants, and diffusion coefficients are required to predict the interfacial pH and flux of the cocrystal components. These values can be obtained independently. The solubility products of the model cocrystals, the ionization constants of their coformers, and the diffusion coefficients in water are summarized in Table 1 for carbamazepine−saccharin (CBZ-SAC) and carbamazepine−salicylic acid (CBZ-SLC). The solubility product of CBZ-SLC was determined by measuring the eutectic concentrations of the components as a function of surfactant concentration. The solubility product of CBZ-SAC was obtained from the literature.[13] The diffusion coefficients in water were estimated using the approach of Othmer and Thakar.[33] According to Othmer and Thakar's equation for estimating diffusion in dilute water solutions, the aqueous diffusion coefficient is inversely proportional to the molecular volume of the substance.[33] CBZ being a larger molecule, its diffusion coefficient in water is smaller than that of both SAC and SLC.

Table 1. Physicochemical Properties of Model Cocrystals and Their Components

			aq diffusion coeff[c] ($\times 10^{-6}$ cm^2/s)	
cocrystal (R-HA)	K_{sp} (mM^2)	pK_a of HA	$D_{R_{aq}}$	$D_{HA_{aq}}$
CBZ-SAC	1.00[a]	1.6[a]	5.7	7.6
CBZ-SLC	0.40	3.0[b]	5.7	7.7

[a]From ref 13. [b]From ref 17. [c]Estimated using Othmer and Thakar's equation.[33]

The micellar solubilization constants of the drug and coformers are summarized in Table 2. The solubilization power of a surfactant can be influenced by the size and shape of the micelles.[34,35] It was reported in the literature that the size and shape of the micelles may change as surfactant and additive concentrations change.[36] Therefore, it was not surprising to observe that SLS solubilizes CBZ to different extents at different concentrations. The solubilization of coformers in SLS is small compared to that of the drug, and the K_s values were assumed to be independent of SLS concentration in the range studied. The diffusion of CBZ in SLS solution would be smaller than that of the coformers because CBZ is significantly solubilized in the micelles compared to both SAC and SLC.

Solubility Study. The concentrations of the cocrystal components at the eutectic point are shown in Figure 4 for both cocrystals at pH 1 as a function of SLS concentration. Since all the experiments were performed above the CSC, the eutectic concentrations of the drug were greater than those of the coformers, meaning the solubility of the cocrystal is less than that of the drug under these conditions. At the eutectic point, the solid phases of both drug and cocrystal are in equilibrium with solution, and thus the drug eutectic concentration is at its solubility at the same solution conditions.[27] This allows the calculations of solubilization constants for the drug shown in Table 2. Using a previously developed model,[27] the solubility of CBZ-SAC and CBZ-SLC was determined from the eutectic concentrations and plotted in Figure 5. The lowest SLS concentration used was 22 mM, which is above the reported CMC of SLS in the literature (6 mM).[17] The formation of micelles in solution preferentially solubilizes CBZ and results in solubility enhancement as SLS concentration increases. SLS does not solubilize SAC and SLC to the same extent as CBZ because these coformers are more hydrophilic. The differential solubilization between the drug and coformers causes the solubility of the cocrystal to increase nonlinearly as a function of surfactant concentration, and the slightly nonlinear nature of the curves in Figure 5 may be attributed to this.

Table 2. Micellar Solubilization Constants of CBZ, SAC, and SLC in SLS Solution

	K_s in SLS (mM^{-1})					
components	22−44 mM	70 mM	100 mM	150 mM	250 mM	400 mM
CBZ	0.58[a]	0.465[b] ± 0.004	0.45[b] ± 0.01	0.43[b] ± 0.01	0.392[b] ± 0.003	0.35[b] ± 0.01
SAC	0.013[a]					
SLC	0.060[a]					

[a]From ref 17. The K_s values for SAC and SLC are assumed to be constant for SLS concentrations ranging from 22 to 400 mM. [b]Determined using $S_T = S_{aq}(1 + K_s^R[m])$, where S_T is the total solubility of the drug in SLS solution and S_{aq} is the aqueous solubility in water, which is 0.53 mM.[17] The total drug solubility in SLS solution is the same as the eutectic concentrations of CBZ shown in Figure 4 because both solid drug and cocrystal are in equilibrium with solution at the eutectic point.[27]

DOI: 10.1021/acs.molpharmaceut.5b00862
Mol. Pharmaceutics 2016, 13, 1030−1046

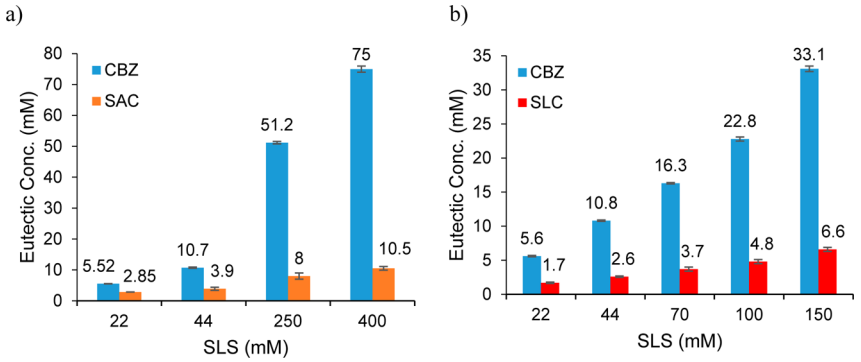

Figure 4. Eutectic measurements for CBZ-SAC (a) and CBZ-SLC (b) at pH 1 as a function of SLS concentration.

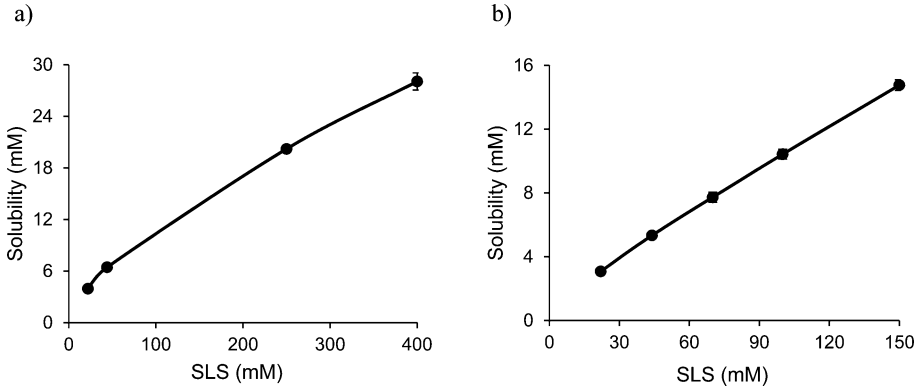

Figure 5. Solubility of cocrystals CBZ-SAC (a) and CBZ-SLC (b) at pH 1 as a function of surfactant concentration. Cocrystal solubility was determined using eutectic concentrations from Figure 4 by $S_{cc} = \sqrt{[\text{drug}]_{\text{eutectic}}[\text{coformer}]_{\text{eutectic}}}$.[27]

Effect of Surfactant on Dissolution. The dissolution profiles of CBZ-SAC and CBZ-SLC at different SLS concentrations at constant pH (pH = 1) where the coformers are mostly nonionized are shown in Figure 6. Since experiments were conducted above the CSC where the cocrystals were thermodynamically stable, the dissolution behavior of both cocrystals was linear as expected under sink conditions. Similar to solubility, the dissolution rates of both cocrystals increase as SLS concentration increases.

The effective diffusion coefficients of CBZ can be estimated from the dissolution rates of the cocrystals at pH 1 as a function of SLS concentration using eq 63 in the Appendix. The micellar diffusivity of CBZ can then be estimated from the effective diffusivity according to the following relationship:

$$D_{R_{eff}} = \frac{D_{aq} + K_s D_m[m]}{1 + K_s[m]} \quad (14)$$

where $D_{R_{eff}}$ is the effective diffusivity of the drug and D_m is the micellar diffusivity.[37] The micellar diffusivities of CBZ for the two cocrystals as a function of SLS concentration are plotted in Figure 7. A power regression can be fitted to describe the relationship between micellar diffusivity and SLS concentration. Micellar diffusivity of CBZ decreases as surfactant concentration increases. The same trend was also observed in the literature.[38−40] Detailed analysis of this is beyond the scope of this study. However, this behavior may be due to the formation of larger micelles as surfactant concentration increases[38] and the potential changes in viscosity. Another possible reason could be the increase in electrostatic repulsion as surfactant concentration increases since SLS is negatively charged.[39] The diffusion of the micelle−drug complexes can be reduced by the electronic repulsion between the negatively charged micelles.[39] The CBZ micellar diffusivities determined from the dissolution of CBZ-SLC are somewhat greater than those determined for CBZ-SAC. The reason for these differences is not known, but they may be due to the different chemical environments surrounding the micelles between the two cocrystals. Both SAC and SLC are able to ionize and form negatively charged ions that can potentially increase the electronic repulsion in solution. CBZ-SAC has a higher K_{sp} value and SAC is more acidic than SLC, so the degree of SAC ionization is higher than that of SLC at the same pH. The higher SAC ion concentration in solution may cause a greater increase in electronic repulsion for CBZ-SAC than CBZ-SLC. Consequently, the diffusion of micelles may be slower in CBZ-SAC dissolution than in CBZ-SLC dissolution. For this study, the micellar diffusivities shown in Figure 7 are used to assess the mass transport models described here. It is also appropriate to point out that eq 63 does not take into account kinetic processes involving surfactant and micelles that may occur at the dissolving surface.

Effect of pH on Dissolution. The effect of pH on dissolution of cocrystals was studied at constant surfactant concentration as a function of pH. The dissolution experiments were conducted in 400 mM SLS solution for CBZ-SAC and 150 mM for CBZ-SLC. The dissolution profiles of CBZ-SAC and CBZ-SLC in terms of cocrystal components as a function of pH are shown in Figures 8 and 9. The linear dissolution behavior of the two cocrystals indicates that no solid phase transformation occurred during dissolution as the experiments were performed above the CSC. The dissolution rates of both cocrystals increase as pH increases and then remain relatively

DOI: 10.1021/acs.molpharmaceut.5b00862
Mol. Pharmaceutics 2016, 13, 1030−1046

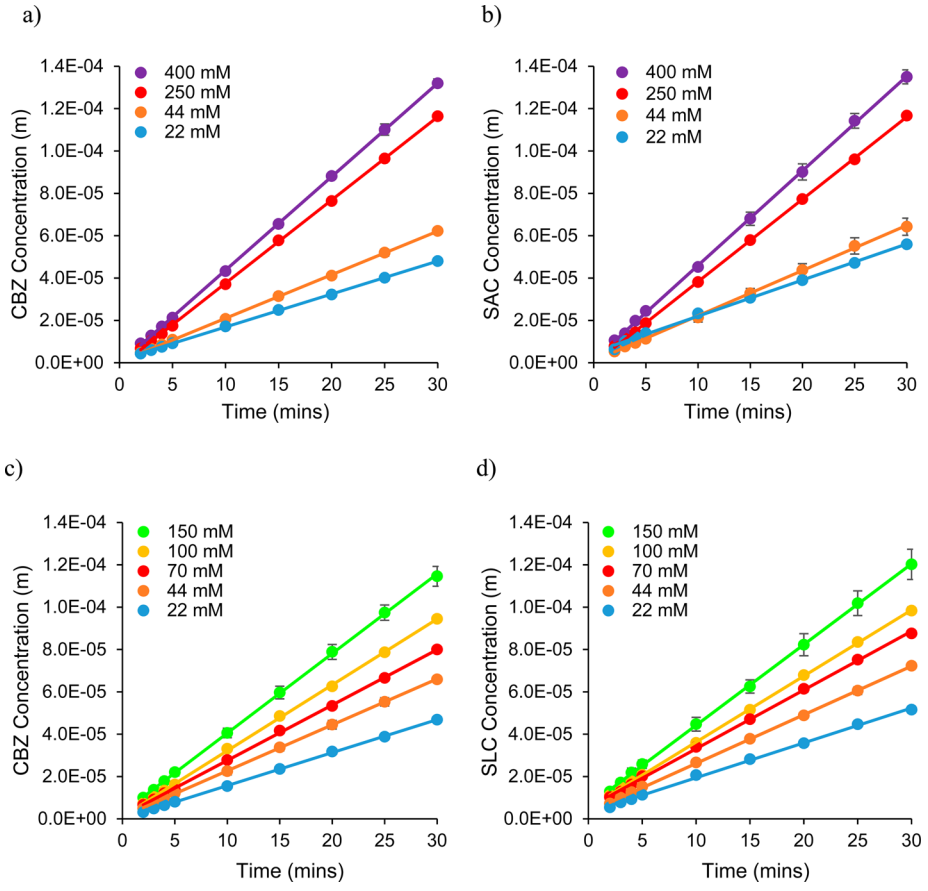

Figure 6. Dissolution profiles for CBZ-SAC in terms of CBZ concentrations (a) and SAC concentrations (b); and CBZ-SLC in terms of CBZ concentrations (c) and SLC concentrations (d) at different SLS concentrations at pH 1. The solid circles are experimental data points, and the solid lines are fitted linear regressions.

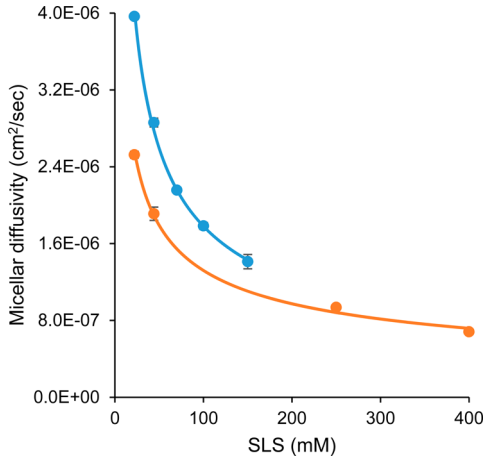

Figure 7. Micellar diffusivities of CBZ determined from the dissolution of CBZ-SAC (orange line) and CBZ-SLC (blue line) at pH 1 as a function of SLS concentration. The solid circles are experimental data points determined from the dissolution shown in Figure 6 using eqs 63 and 14 and solubility data shown in Figure 5. The solid lines are the fitted power regression. The power regression line for CBZ-SAC is $y = 9.977 \cdot 10^{-6}\, x^{-0.439}$ and for CBZ-SLC is $y = 2.155 \cdot 10^{-5}\, x^{-0.542}$.

constant in the self-buffering region of the coformers. Since SAC has a lower pK_a than SLC, pH has a greater impact on the dissolution rate of CBZ-SAC compared to CBZ-SLC as reflected in the larger range of dissolution rates in Figure 8 compared to Figure 9.

Comparison of Flux Predictions between the Mass Transport Models. For comparison purposes, only literature reported micellar diffusivities of CBZ in SLS solution were used and no parameters were adjusted to fit the experimental data to the theoretical equations of the two transport models shown in Table 3 and Figure 10. A micellar diffusivity of 3.6×10^{-7} cm^2/s at 400 mM SLS was used for CBZ-SAC, and for CBZ-SLC, a value of 6.4×10^{-7} cm^2/s at 150 mM SLS was used.[40] The difference in concentrations of the cocrystal components at the surface predicted using the two models and how this difference could affect the interfacial pH are illustrated in Table 3 for the dissolution of CBZ-SAC at 400 mM SLS. The interfacial pH calculated from both models lags behind bulk pH above the pK_a value of SAC (pK_a = 1.6) due to the ionization of SAC in the diffusion layer. The interfacial equilibrium model predicts a lower surface pH (approximately 0.3 pH unit at pH 6) compared to the surface saturation model. The lower interfacial pH calculated from the interfacial equilibrium model is due to the greater SAC concentration predicted at the dissolving surface to maintain the K_{sp} of CBZ-SAC. As shown in Table 3, the concentrations of both CBZ and SAC at the surface calculated from the interfacial equilibrium model are higher than those calculated from the surface saturation model. Because of the depletion of SAC at the surface of the boundary layer due to faster diffusion, the concentration product of CBZ and SAC from the surface saturation model is less than the K_{sp} of CBZ-SAC. In order to re-establish the equilibrium disrupted by diffusion, both CBZ and SAC concentrations from the

DOI: 10.1021/acs.molpharmaceut.5b00862
Mol. Pharmaceutics 2016, 13, 1030−1046

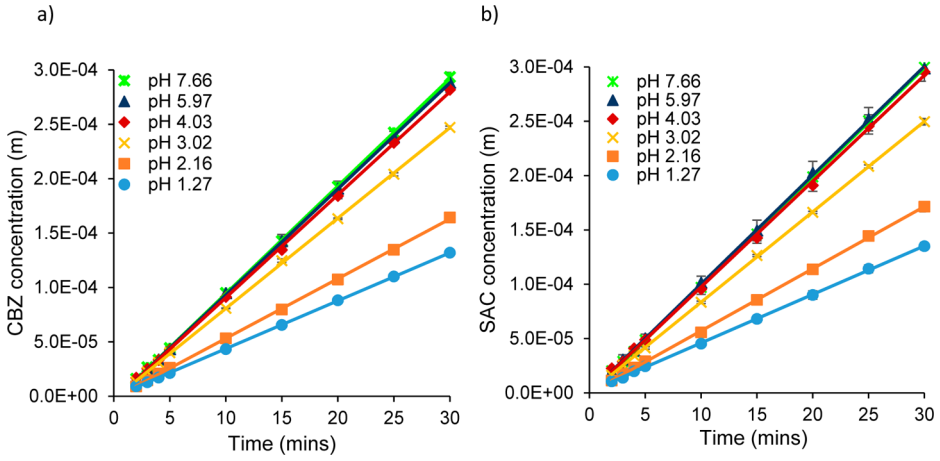

Figure 8. Dissolution profiles of CBZ-SAC in terms of CBZ (a) and SAC (b) as a function of bulk pH at 400 mM SLS. The symbols are experimental data points, and the solid lines are fitted linear regressions. The pH values represent the initial bulk pH of the dissolution media.

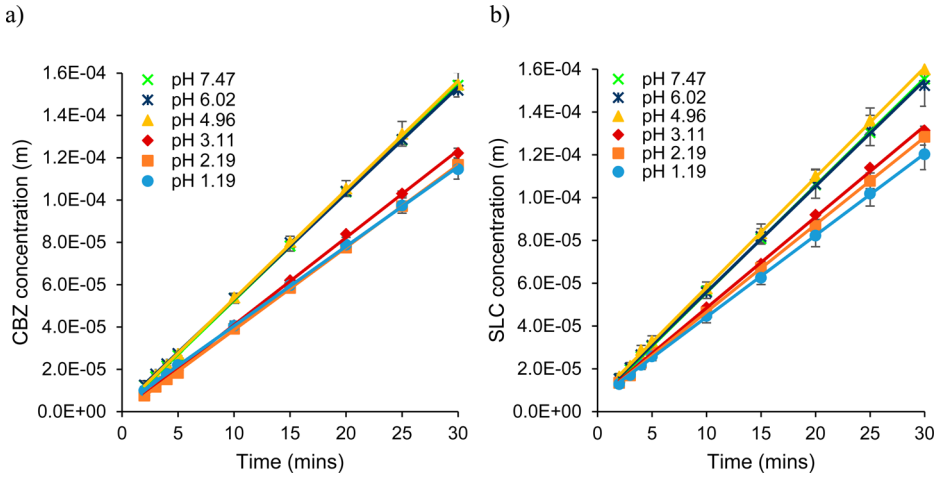

Figure 9. Dissolution profiles of CBZ-SLC in terms of CBZ (a) and SLC (b) as a function of bulk pH at 150 mM SLS. The symbols are experimental data points, and the solid lines are fitted linear regressions. The pH values represent the initial bulk pH of the dissolution media.

interfacial equilibrium model are predicted to increase at the surface to maintain a concentration product equal to the K_{sp} of CBZ-SAC. As seen in Table 3 and Figure 10, both models result in qualitatively similar predictions. Subtle but potentially important differences in surface concentrations result in different predicted dissolution rates.

The flux of CBZ-SAC at 400 mM SLS and CBZ-SLC at 150 mM SLS as a function of bulk pH was predicted using both models, and the predicted values were compared with the experimental data as shown in Figure 10. The predictions from both models follow the same trend as the experimental data. However, the predictions from both models deviate from the experimental data because the effective diffusivities of CBZ used here were estimated from the micellar diffusivities of SLS in the literature determined at conditions different from the study here. The surface saturation model slightly underpredicted the flux, while the interfacial equilibrium model overpredicted the flux. However, the surface saturation model is able to provide more accurate prediction of cocrystal flux compared to the interfacial equilibrium model. It is difficult to experimentally prove which model more accurately represents the conditions at the dissolving surface as it requires concentration measurements at the dissolving surface. Analysis of the experimental results and theoretical predictions from the surface saturation model indicated somewhat better alignment. Consequently, the surface saturation model is used to perform the mass transport analysis for the two cocrystals studied here.

Interfacial pH and CSC Predictions from Surface Saturation Model. Interfacial pH can be predicted using eq 59 derived from the surface saturation model shown in the Appendix and the physicochemical parameters of the cocrystals and their components (e.g., solubility products, ionization constants, solubilization constants, and effective diffusivities). The effect of bulk pH and surfactant concentration on interfacial pH for CBZ-SAC and CBZ-SLC is shown in Figure 11 utilizing the surface saturation model. At constant surfactant concentration, for bulk pH < pK_a, interfacial pH is approximately equal to bulk pH because the hydrogen ion in the bulk solution suppresses the ionization of the coformers.[24] As bulk pH increases above the pK_a value of the coformer, coformer ionization begins to occur. This, in effect, results in a buffer effect at the interface, and the interfacial pH no longer continues to increase linearly with increasing bulk pH.[24] Both cocrystals have the ability to self-buffer the pH microenvironment in the diffusion layer,[24] and this is demonstrated by the plateau region that ranges from bulk pH 4 to 8 in Figure 11. CBZ-SAC is able to self-buffer the interfacial pH to around 3.0; while the plateau interfacial pH for CBZ-SLC is around 3.7.

DOI: 10.1021/acs.molpharmaceut.5b00862
Mol. Pharmaceutics 2016, 13, 1030−1046

Table 3. Interfacial pH and Concentrations of CBZ and SAC at the Surface Calculated Using the Surface Saturation and Interfacial Equilibrium Models for the Dissolution of CBZ-SAC at 400 mM SLS as a Function of Bulk pH

		concs at the surface (mM)				
bulk pH	interfacial pH[a]	$[CBZ]_{tot}$[b]	$[CBZ]_{aq}$[c]	$[SAC]_{tot}$[d]	$[SAC]_{aq}$[e]	$[CBZ]_{aq} \times [SAC]_{aq}$ (mM^2)
			Surface Saturation Model			
1.27	1.27	30.4	0.2	4.2	0.6	0.1
2.16	2.15	36.8	0.3	5.1	0.5	0.1
3.02	2.84	57.4	0.4	8.0	0.3	0.1
4.03	3.10	72.7	0.5	10.1	0.3	0.1
5.97	3.14	75.6	0.5	10.5	0.3	0.1
7.66	3.14	75.6	0.5	10.5	0.3	0.1
			Interfacial Equilibrium Model			
1.27	1.27	81.5	0.6	11.3	1.7	1.0
2.16	2.14	98.3	0.7	13.7	1.4	1.0
3.02	2.70	137.3	1.0	19.1	1.0	1.0
4.03	2.85	155.2	1.1	21.6	0.9	1.0
5.97	2.87	157.9	1.1	22.0	0.9	1.0
7.66	2.87	157.9	1.1	22.0	0.9	1.0

[a]Calculated using eq 59 for surface saturation model and eq 71 for interfacial equilibrium model with K_{sp}, K_a, K_s, and $D_{HA_{aq}}$ values shown in Tables 1 and 2. $D_{HA_{eff}}$ is assumed to be equal to $D_{HA_{aq}}$. The $D_{R_{eff}}$ value for CBZ-SAC (3.9×10^{-7} cm^2/s) was calculated from eq 14 using the D_m value of 3.6×10^{-7} cm^2/s from the literature.[40] The diffusion coefficients for H^+ and OH^- are 9.31×10^{-5} and 5.28×10^{-5} cm^2/s, respectively.[41] [b]Calculated using eq 27 with the K_s value from Table 2 and calculated $[CBZ]_{aq}$ from surface saturation and interfacial equilibrium models. [c]Calculated using eq 52 for surface saturation model and eq 65 for interfacial equilibrium model. K_{sp}, K_a, and K_s values are from Tables 1 and 2; for interfacial pH, see footnote [a]. $D_{R_{eff}}$ is 3.9×10^{-7} cm^2/s, and $D_{HA_{eff}}$ is assumed to be equal to $D_{HA_{aq}}$ shown in Table 1. [d]Calculated using eq 28 with the K_s and K_a values from Tables 1 and 2, calculated $[SAC]_{aq}$ from surface saturation and interfacial equilibrium models; for interfacial pH, see footnote [a]. [e]Calculated using eq 54 for surface saturation model and eq 66 for interfacial equilibrium model. K_{sp}, K_a, and K_s values are from Tables 1 and 2; for interfacial pH, see footnote [a]. $D_{R_{eff}}$ is 3.9×10^{-7} cm^2/s, and $D_{HA_{eff}}$ is assumed to be $D_{HA_{aq}}$ shown in Table 1.

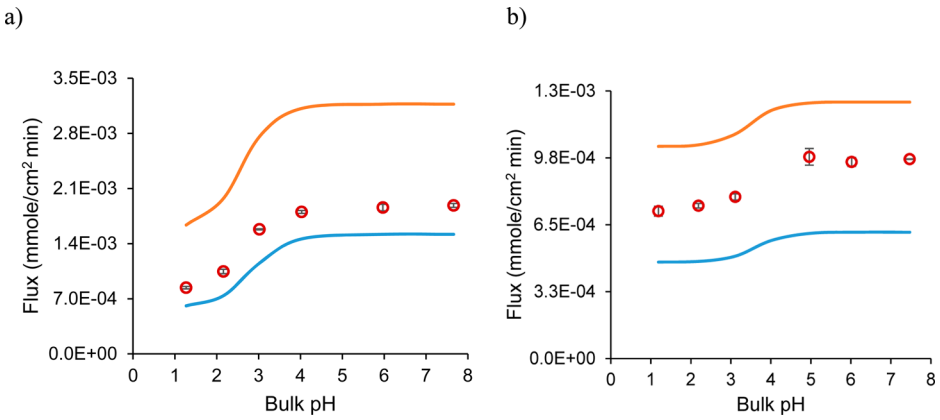

Figure 10. Experimental (red circles) and predicted flux comparison of CBZ-SAC at 400 mM SLS (a) and CBZ-SLC at 150 mM SLS (b) as a function of bulk pH using the surface saturation model (blue line) and interfacial equilibrium model (orange line). The flux was calculated using eqs 63 and 72 based on the interfacial pH predicted from eqs 59 and 71 for surface saturation and interfacial equilibrium models, respectively. The K_{sp}, K_a, K_s, and $D_{HA_{aq}}$ values are shown in Tables 1 and 2. $D_{R_{eff}}$ value for CBZ-SAC is 3.9×10^{-7} cm^2/s and for CBZ-SLC is 7.2×10^{-7} cm^2/s.

The buffering ability is affected by the degree of ionization of the ionizable components at the interface, and this is determined by the concentrations and pK_a values of the ionizable components. With a higher solubility product and a lower pK_a, CBZ-SAC is able to self-buffer to a lower pH at the interface compared to CBZ-SLC. Surfactant has little or no effect on interfacial pH at bulk pH < pK_a values of the coformers because the interfacial pH is determined by bulk pH. As bulk pH increases above the pK_a of the coformer, the degree of coformer ionization is not affected by SLS significantly enough to cause any changes in interfacial pH. For the cocrystals studied here, no significant impact on interfacial pH was predicted or observed as a function of surfactant concentration.

The critical stabilization concentration, CSC, has a pH dependence for the cocrystals studied here, so different surfactant concentrations will be required to stabilize the cocrystals at different pH to prevent solid phase transformation. Based on the predicted interfacial pH, the CSC needed at the dissolving cocrystal surface to prevent phase transformation can be estimated using the previously developed model.[17] The surfactant concentrations that are required to stabilize the model cocrystals at different pH are calculated and shown in Table 4.

The CSC of CBZ-SAC is significantly higher than that of CBZ-SLC since the solubility of CBZ-SAC is higher and thus requires higher surfactant concentration to stabilize the cocrystal during dissolution. Because of the self-buffering ability

DOI: 10.1021/acs.molpharmaceut.5b00862
Mol. Pharmaceutics 2016, 13, 1030−1046

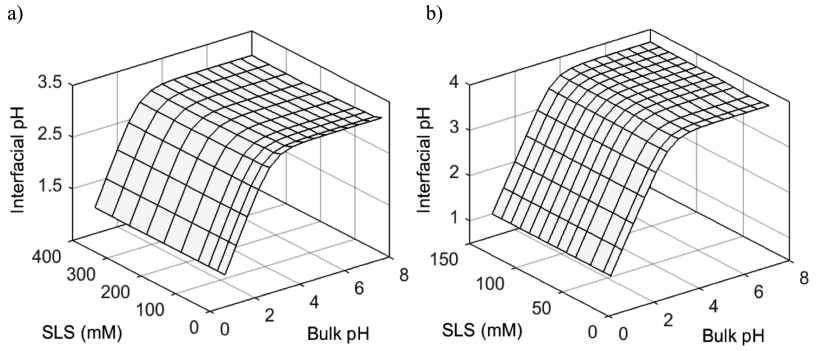

Figure 11. Theoretical predictions of interfacial pH for CBZ-SAC (a) and CBZ-SLC (b) as a function of pH and SLS concentration using surface saturation model. Interfacial pH was calculated using eq 59. The K_{sp}, K_a, K_s, and $D_{HA_{aq}}$ values are shown in Tables 1 and 2, and $D_{R_{eff}}$ values are from Figure 7.

Table 4. Estimated SLS Concentrations for Stabilizing Cocrystals during Dissolution at Different pH Using the Surface Saturation Model

CBZ-SAC			CBZ-SLC		
pH			pH		
bulk	interfacial[a]	CSC[b] (mM)	bulk	interfacial[a]	CSC[b] (mM)
1.0	1.0	12	1.0	1.0	7
2.0	2.0	27	2.0	2.0	7
3.0	2.8	161	3.0	3.0	10
4.0	3.0	306	4.0	3.6	18
5.0	3.0	326	5.0	3.7	21
6.0	3.0	326	6.0	3.7	21
7.0	3.0	326	7.0	3.7	21
8.0	3.0	326	8.0	3.7	21

[a]From Figure 11. [b]Calculated from previously developed model.[17]

of the cocrystals, the CSC is essentially the same in the buffering region regardless of the bulk pH.

Surface Saturation Model Flux Predictions: pH effect. The flux of the cocrystals was calculated from the dissolution rates and compared to theoretical predictions to evaluate the predictive power of the surface saturation model. The theoretical flux can be calculated using eq 63 in the Appendix and the physicochemical parameters of the cocrystals and their components. The experimental and theoretical flux comparison is shown in Figure 12. The experimental data confirmed that the flux values of the cocrystal components are equal as expected because the stoichiometry of both cocrystals is 1:1. Also as expected, the fluxes of CBZ-SAC and CBZ-SLC plateau in the buffering region because there is minimal change in interfacial pH as predicted from the mass transport analysis. By modeling the interfacial pH, the theoretical flux shows excellent agreement with the experimental data using the physicochemical parameters in Tables 1 and 2 and Figure 7. Because of the acidity of SAC, the flux of CBZ-SAC is very sensitive to interfacial pH changes, and this can lead to the large deviations observed in the buffering region. A 0.2 unit pH change in interfacial pH around 3.0 can lead to a roughly 20% change in the flux of CBZ-SAC. Accurate predictions of interfacial pH are clearly very important for predicting the flux of cocrystals with ionizable components.

Combination Effect of pH and Surfactant on Dissolution. The combination of pH and surfactant effect on the dissolution of cocrystals was studied by performing dissolution experiments at different pH and surfactant concentrations. The dissolution rates were expressed in terms of flux and compared to the predicted values from the surface saturation model. The dependence of flux on pH and surfactant concentration for both cocrystals is shown in the three-dimensional plots in Figure 13. For both cocrystals, the theoretical values showed excellent agreement with the experimental data. There are fewer experimental data points on the CBZ-SAC plot because much of the area in the plot is

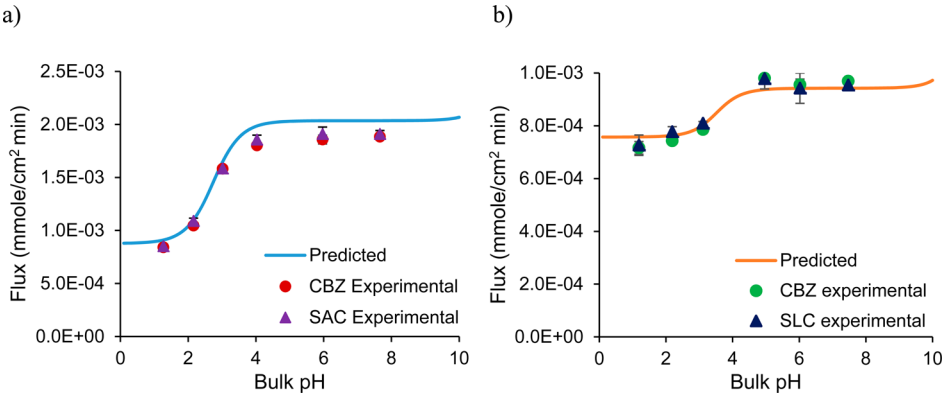

Figure 12. Flux of CBZ-SAC at 400 mM SLS (a) and CBZ-SLC at 150 mM SLS (b) as a function of bulk pH. Flux predictions were calculated using eq 63 based on the interfacial pH predicted from Figure 11. The K_{sp}, K_a, and K_s values are shown in Tables 1 and 2, and $D_{R_{eff}}$ values are from Figure 7.

DOI: 10.1021/acs.molpharmaceut.5b00862
Mol. Pharmaceutics 2016, 13, 1030−1046

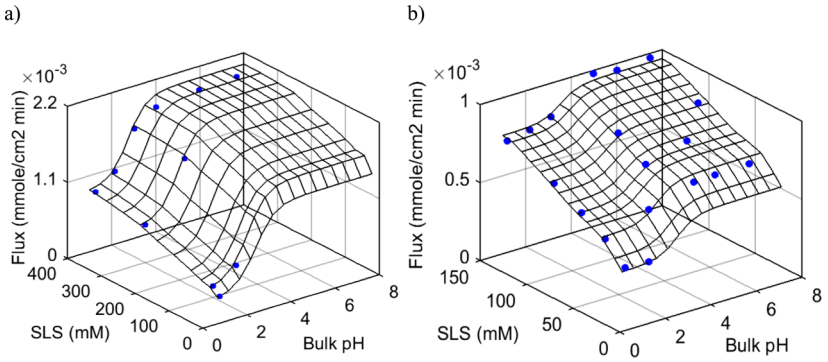

Figure 13. Influence of pH and surfactant concentration on flux of CBZ-SAC (a) and CBZ-SLC (b). The wireframe mesh represents the theoretical flux predictions, and circles represent the experimentally measured flux of cocrystals in terms of CBZ. Flux predictions were calculated using eq 63 based on the interfacial pH predicted from Figure 11. The K_{sp}, K_a, and K_s values are shown in Tables 1 and 2, and $D_{R_{eff}}$ values are from Figure 7.

not experimentally accessible due to the potential phase transformation during dissolution. At the buffering region (bulk pH 4 to 8), the surfactant concentration required to stabilize CBZ-SAC during dissolution is at least 326 mM (Table 4). Due to the potential conversion of CBZ-SAC back to the stable drug form, no dissolution experiments were performed in SLS concentration below 400 mM in the bulk pH range of 4 to 8. The effect of bulk pH on the flux of cocrystal is dictated by the interfacial pH. Any bulk pH change in the range of 4 to 8 does not have a significant impact on the dissolution of the cocrystal because the cocrystal can self-buffer the pH microenvironment at the dissolving surface to produce essentially the same interfacial pH. Flux increases as surfactant concentration increases; however, the increase is larger at lower surfactant concentration.

The effects of surfactant concentration on solubility and micellar diffusivity are opposite. At low surfactant concentrations, the advantage of solubility enhancement on dissolution is greater than the disadvantage of decreased micellar diffusivity, so the increase in flux is greater. As surfactant concentration increases, the disadvantage of reduced micellar diffusivity is slowly approaching the advantage of solubility enhancement, and thus the flux increase is smaller. When the opposite effects of surfactant on micellar diffusivity and solubility essentially cancel each other out, the enhancement in flux by surfactant is limited as indicated by the plateau values of CBZ-SAC at surfactant concentrations ranging from 300 to 400 mM.

DISCUSSION

This work highlights the importance of interfacial pH in determining the flux of cocrystals with ionizable components. Without the knowledge of interfacial pH, one might assume that the pH at the dissolving surface is the same as the bulk pH. Assuming this, the flux of both CBZ-SAC and CBZ-SLC would be expected to increase with increasing bulk pH instead of plateauing at the buffering region. The fifth order equation (eq 59) developed from the mass transport analysis of the surface saturation model gives reasonably accurate predictions of interfacial pH that are otherwise difficult to measure experimentally. This allows the model to capture the plateaued region in the flux of both cocrystals as a function of bulk pH. The surfactant concentrations required to stabilize the cocrystal during dissolution at different bulk pH can also be estimated from the interfacial pH predictions. The use of surfactant can enhance the dissolution of cocrystals, but sometimes the enhancement may not be as large as expected because of the counterbalancing effect of surfactant on solubility and micellar diffusion coefficients.

One of the important elements for the mass transport analysis of cocrystal is the concentrations of the cocrystal components at the dissolving surface as they determine the rate of dissolution. The surface concentrations of the components may not follow the cocrystal's stoichiometric ratio because they have different diffusion coefficients. For the cocrystals studied here, the drug has a slower diffusion compared to the coformers. According to the surface saturation model, the slower diffusing component (i.e., the drug) is able to maintain a surface concentration at the stoichiometric cocrystal solubility and acts as the determinant for the dissolution of the cocrystal while the faster diffusing component has a lower surface concentration. The mass transport analysis here is only applicable for cocrystals that have the same stoichiometry and ionization property as CBZ-SAC and CBZ-SLC. However, the surface saturation model developed here can be applied to the mass transport analysis for cocrystals with different stoichiometries and ionization properties.

CONCLUSIONS

The mechanism of cocrystal dissolution as a function of pH and surfactant concentration has been successfully analyzed through the development and evaluation of a physically realistic mass transport model. This mass transport analysis demonstrated the importance of interfacial pH in determining the flux of cocrystals with ionizable components. The ionizable components have the ability to self-buffer the pH microenvironment at the interface. Evaluation of the physicochemical properties, such as solubility product, ionization constant, solubilization constant, and diffusion coefficient, are required for accurate prediction of interfacial pH and flux of the cocrystal. The predictive power of the mass transport analysis was evaluated by performing dissolution above the CSC to prevent the conversion of highly soluble cocrystal back to the drug form. The model adequately describes the dissolution behavior of cocrystal as a function of pH and surfactant concentration. Bulk pH itself does not adequately explain the dissolution behavior of cocrystal because the rate of dissolution is affected by the pH at the interface. The effect of surfactant on dissolution of cocrystal is also an important consideration and can diminish as surfactant concentration increases due to the counterbalancing effects of surfactant on micellar diffusivity and solubility.

DOI: 10.1021/acs.molpharmaceut.5b00862
Mol. Pharmaceutics 2016, 13, 1030−1046

APPENDIX

The chemical equilibria and the equations for equilibrium constants during the dissolution of 1:1 cocrystal, RHA, with R as the nonionizable drug and HA as the weak acidic coformer in the presence of surfactant can be described as follows:

$$(\mathrm{RHA})_{\mathrm{solid}} \leftrightharpoons \mathrm{R}_{\mathrm{aq}} + \mathrm{HA}_{\mathrm{aq}} \tag{15}$$

$$K_{\mathrm{sp}} = [\mathrm{R}]_{\mathrm{aq}}[\mathrm{HA}]_{\mathrm{aq}} \tag{16}$$

$$\mathrm{R}_{\mathrm{aq}} + \mathrm{m} \leftrightharpoons \mathrm{R}_{\mathrm{m}} \tag{17}$$

$$K_{\mathrm{s}}^{\mathrm{R}} = \frac{[\mathrm{R}]_{\mathrm{m}}}{[\mathrm{R}]_{\mathrm{aq}}[\mathrm{m}]} \tag{18}$$

$$\mathrm{HA}_{\mathrm{aq}} + \mathrm{m} \leftrightharpoons \mathrm{HA}_{\mathrm{m}} \tag{19}$$

$$K_{\mathrm{s}}^{\mathrm{HA}} = \frac{[\mathrm{HA}]_{\mathrm{m}}}{[\mathrm{HA}]_{\mathrm{aq}}[\mathrm{m}]} \tag{20}$$

$$\mathrm{H_2O} + \mathrm{HA}_{\mathrm{aq}} \leftrightharpoons \mathrm{H_3O^+} + \mathrm{A}_{\mathrm{aq}}^- \tag{21}$$

$$K_{\mathrm{a}} = \frac{[\mathrm{H_3O^+}][\mathrm{A}^-]_{\mathrm{aq}}}{[\mathrm{HA}]_{\mathrm{aq}}} \tag{22}$$

$$\mathrm{H_3O^+} + \mathrm{OH}^- \leftrightharpoons 2\mathrm{H_2O} \tag{23}$$

$$K_{\mathrm{w}} = [\mathrm{H_3O^+}][\mathrm{OH}^-] \tag{24}$$

$$\mathrm{HA}_{\mathrm{aq}} + \mathrm{OH}^- \leftrightharpoons \mathrm{H_2O} + \mathrm{A}_{\mathrm{aq}}^- \tag{25}$$

$$K_{\mathrm{l}} = \frac{[\mathrm{A}^-]_{\mathrm{aq}}}{[\mathrm{HA}]_{\mathrm{aq}}[\mathrm{OH}^-]} \tag{26}$$

where $K_{\mathrm{s}}^{\mathrm{R}}$ is the solubilization constant of R and $K_{\mathrm{s}}^{\mathrm{HA}}$ is the solubilization constant of HA, [m] is the micellar concentration in the solution and is equal to the total surfactant concentration minus the CMC, K_{a} is the ionization constant of HA, K_{w} is the dissociation constant of water, and K_{l} is the ratio of $K_{\mathrm{a}}/K_{\mathrm{w}}$. Subscript aq denotes the aqueous phase, and m denotes the micellar phase. An assumption in this analysis is that the ionized coformer is not solubilized by surfactant.

The total concentrations of the cocrystal components, $[\mathrm{R}]_{\mathrm{tot},0}$ and $[\mathrm{A}]_{\mathrm{tot},0}$, at the dissolving surface can be described as

$$[\mathrm{R}]_{\mathrm{tot},0} = [\mathrm{R}]_{\mathrm{aq},0}(1 + K_{\mathrm{s}}^{\mathrm{R}}[\mathrm{m}]) \tag{27}$$

$$[\mathrm{A}]_{\mathrm{tot},0} = [\mathrm{HA}]_{\mathrm{aq},0}\left(1 + \frac{K_{\mathrm{a}}}{\mathrm{H}_0^+} + K_{\mathrm{s}}^{\mathrm{HA}}[\mathrm{m}]\right) \tag{28}$$

When the cocrystal is in equilibrium with solution at the dissolving surface at time = 0 before any diffusion, the stoichiometric solubility of RHA is as follows:

$$\begin{aligned} S_{\mathrm{cc}} &= [\mathrm{R}]_{\mathrm{tot},0} \\ &= [\mathrm{A}]_{\mathrm{tot},0} \\ &= \sqrt{K_{\mathrm{sp}}(1 + K_{\mathrm{s}}^{\mathrm{R}}[\mathrm{m}])\left(1 + \frac{K_{\mathrm{a}}}{\mathrm{H}_0^+} + K_{\mathrm{s}}^{\mathrm{HA}}[\mathrm{m}]\right)} \end{aligned} \tag{29}$$

The flux of all the species across the diffusion layer includes both the diffusion and chemical reactions happening during dissolution. At steady state, the diffusion and simultaneous chemical reactions of the individual species within the diffusion layer can be written using Fick's law as follows:[24]

$$\frac{\partial[R]_{\mathrm{aq}}}{\partial t} = D_{\mathrm{R}_{\mathrm{aq}}}\frac{\partial^2[\mathrm{R}]_{\mathrm{aq}}}{\partial x^2} + \phi_1 = 0 \tag{30}$$

$$\frac{\partial[\mathrm{R}]_{\mathrm{m}}}{\partial t} = D_{\mathrm{R}_{\mathrm{m}}}\frac{\partial^2[\mathrm{R}]_{\mathrm{m}}}{\partial x^2} + \phi_2 = 0 \tag{31}$$

$$\frac{\partial[\mathrm{HA}]_{\mathrm{aq}}}{\partial t} = D_{\mathrm{HA}_{\mathrm{aq}}}\frac{\partial^2[\mathrm{HA}]_{\mathrm{aq}}}{\partial x^2} + \phi_3 = 0 \tag{32}$$

$$\frac{\partial[\mathrm{A}^-]_{\mathrm{aq}}}{\partial t} = D_{\mathrm{A}_{\mathrm{aq}}^-}\frac{\partial^2[\mathrm{A}^-]_{\mathrm{aq}}}{\partial x^2} + \phi_4 = 0 \tag{33}$$

$$\frac{\partial[\mathrm{HA}]_{\mathrm{m}}}{\partial t} = D_{\mathrm{HA}_{\mathrm{m}}}\frac{\partial^2[\mathrm{HA}]_{\mathrm{m}}}{\partial x^2} + \phi_5 = 0 \tag{34}$$

$$\frac{\partial[\mathrm{OH}^-]}{\partial t} = D_{\mathrm{OH}^-}\frac{\partial^2[\mathrm{OH}^-]}{\partial x^2} + \phi_6 = 0 \tag{35}$$

$$\frac{\partial[\mathrm{H}^+]}{\partial t} = D_{\mathrm{H}^+}\frac{\partial^2[\mathrm{H}^+]}{\partial x^2} + \phi_7 = 0 \tag{36}$$

where ϕ_{1-7} are the reaction rate functions. At equilibrium, the reaction rate of the reactant should be the opposite of that of the product. Based on the chemical equilibria, the followings can be written as:

$$\phi_1 = -\phi_2 \tag{37}$$

$$\phi_3 = -\phi_4 - \phi_5 \tag{38}$$

The reaction rate of A^- can be reflected by the reaction rate of H^+ and OH^-, therefore,

$$\phi_4 = \phi_7 - \phi_6 \tag{39}$$

Based on eq 39, eq 38 can be written as

$$\phi_3 = \phi_6 - \phi_5 - \phi_7 \tag{40}$$

Based on eqs 37, 38, and 40, the following mass balance equations can be written:

$$D_{\mathrm{R}_{\mathrm{aq}}}\frac{\mathrm{d}^2[\mathrm{R}]_{\mathrm{aq}}}{\mathrm{d}x^2} = -D_{\mathrm{R}_{\mathrm{m}}}\frac{\mathrm{d}^2[\mathrm{R}]_{\mathrm{m}}}{\mathrm{d}x^2} \tag{41}$$

$$D_{\mathrm{HA}_{\mathrm{aq}}}\frac{\mathrm{d}^2[\mathrm{HA}]_{\mathrm{aq}}}{\mathrm{d}x^2} = -D_{\mathrm{A}_{\mathrm{aq}}^-}\frac{\mathrm{d}^2[\mathrm{A}^-]_{\mathrm{aq}}}{\mathrm{d}x^2} - D_{\mathrm{HA}_{\mathrm{m}}}\frac{\mathrm{d}^2[\mathrm{HA}]_{\mathrm{m}}}{\mathrm{d}x^2} \tag{42}$$

$$D_{\mathrm{HA}_{\mathrm{aq}}}\frac{\mathrm{d}^2[\mathrm{HA}]_{\mathrm{aq}}}{\mathrm{d}x^2} = D_{\mathrm{OH}^-}\frac{\mathrm{d}^2[\mathrm{OH}^-]}{\mathrm{d}x^2} - D_{\mathrm{H}^+}\frac{\mathrm{d}^2[\mathrm{H}^+]}{\mathrm{d}x^2} - D_{\mathrm{HA}_{\mathrm{m}}}\frac{\mathrm{d}^2[\mathrm{HA}]_{\mathrm{m}}}{\mathrm{d}x^2} \tag{43}$$

Integrating eqs 41 to 43 once gives

$$D_{\mathrm{R}_{\mathrm{aq}}}\frac{\mathrm{d}[\mathrm{R}]_{\mathrm{aq}}}{\mathrm{d}x} = -D_{\mathrm{R}_{\mathrm{m}}}\frac{\mathrm{d}[\mathrm{R}]_{\mathrm{m}}}{\mathrm{d}x} + C_1 \tag{44}$$

DOI: 10.1021/acs.molpharmaceut.5b00862
Mol. Pharmaceutics 2016, 13, 1030−1046

$$D_{HA_{aq}}\frac{d[HA]_{aq}}{dx} = -D_{A^-_{aq}}\frac{d[A^-]_{aq}}{dx} - D_{HA_m}\frac{d[HA]_m}{dx} + C_2 \quad (45)$$

$$D_{HA_{aq}}\frac{d[HA]_{aq}}{dx} = D_{OH^-}\frac{d[OH^-]}{dx} - D_{H^+}\frac{d[H^+]}{dx} - D_{HA_m}\frac{d[HA]_m}{dx} + C_3 \quad (46)$$

Since A^-_{aq} is the product of the reaction between HA and OH^-, so its flux can be reflected by both OH^- and H^+:

$$-D_{A^-_{aq}}\frac{d[A^-]_{aq}}{dx} = D_{OH^-}\frac{d[OH^-]}{dx} - D_{H^+}\frac{d[H^+]}{dx} \quad (47)$$

With this mass balance relationship, it can be seen that

$$C_2 = C_3 \quad (48)$$

Integrating eqs 41 to 43 one more time gives

$$D_{R_{aq}}[R]_{aq} = -D_{R_m}[R]_m + C_1x + C_4 \quad (49)$$

$$D_{HA_{aq}}[HA]_{aq} = -D_{HA_m}[HA]_m - D_{A^-_{aq}}[A^-]_{aq} + C_2x + C_5 \quad (50)$$

$$D_{HA_{aq}}[HA]_{aq} = D_{OH^-}[OH^-] - D_{H^+}[H^+] - D_{HA_m}[HA]_m + C_3x + C_6 \quad (51)$$

Interfacial pH and flux of the species can be evaluated by solving these mass balance equations with the boundary conditions obtained from the surface saturation and interfacial equilibrium models.

Surface Saturation Model

Given that the concentration of the drug is the same as the solubility of the cocrystal at the surface for the surface saturation model, the aqueous concentration of the drug at the surface can be solved using eqs 27 and 29:

$$[R]_{aq,0} = \frac{\sqrt{K_{sp}(1 + K_s^R[m])\left(1 + \frac{K_a}{H_0^+} + K_s^{HA}[m]\right)}}{1 + K_s^R[m]} \quad (52)$$

Assuming the dissolution of RHA in the presence of surfactant gives equal flux of R and HA:

$$J_{R_{tot}} = \frac{D_{R_{eff}}[R]_{tot,0}}{h} = J_{A_{tot}} = \frac{D_{HA_{eff}}[A]_{tot,0}}{h} \quad (53)$$

where $D_{R_{eff}}$ and $D_{HA_{eff}}$ are the effective diffusion coefficients of the drug and coformer, which are defined in eq 14 as the total diffusion of the free and micelle solubilized solute.[37] Given eqs 27−29 above and applying the equation for diffusion layer thickness shown in eq 10, the aqueous concentration of the coformer at the surface is given by

$$[HA]_{aq,0} = \left(\frac{D_{R_{eff}}}{D_{HA_{eff}}}\right)^{2/3} \frac{\sqrt{K_{sp}(1 + K_s^R[m])\left(1 + \frac{K_a}{H_0^+} + K_s^{HA}[m]\right)}}{1 + \frac{K_a}{H_0^+} + K_s^{HA}[m]} \quad (54)$$

Based on eqs 52 and 54, the following boundary conditions for each species can be written for the surface saturation model. At $x = 0$:

$$[R]_{aq,0} = \frac{\sqrt{K_{sp}(1 + K_s^R[m])\left(1 + \frac{K_a}{H_0^+} + K_s^{HA}[m]\right)}}{1 + K_s^R[m]}$$

$$[HA]_{aq,0} = \left(\frac{D_{R_{eff}}}{D_{HA_{eff}}}\right)^{2/3} \frac{\sqrt{K_{sp}(1 + K_s^R[m])\left(1 + \frac{K_a}{H_0^+} + K_s^{HA}[m]\right)}}{1 + \frac{K_a}{H_0^+} + K_s^{HA}[m]}$$

$$[R]_{m,0} = \text{unknown}$$

$$[HA]_{m,0} = \text{unknown}$$

$$[A^-]_{aq,0} = \text{unknown}$$

$$[H^+] = [H^+]_0$$

$$[OH^-] = [OH^-]_0$$

At $x = h$:

$$[R]_{aq,h} = 0 \text{ (under sink condition)}$$

$$[HA]_{aq,h} = 0 \text{ (under sink condition)}$$

$$[R]_{m,h} = 0 \text{ (under sink condition)}$$

$$[HA]_{m,h} = 0 \text{ (under sink condition)}$$

$$[A^-]_{aq,h} = 0 \text{ (under sink condition)}$$

$$[H^+] = [H^+]_h$$

$$[OH^-] = [OH^-]_h$$

Evaluation of pH at the Solid Surface

Applying the above boundary conditions to eqs 50 and 51, at $x = 0$:

$$D_{HA_{aq}}\left(\frac{D_{R_{eff}}}{D_{HA_{eff}}}\right)^{2/3} \frac{\sqrt{K_{sp}(1 + K_s^R[m])\left(1 + \frac{K_a}{H_0^+} + K_s^{HA}[m]\right)}}{1 + \frac{K_a}{H_0^+} + K_s^{HA}[m]} = -D_{HA_m}[HA]_{m,0} - D_{A^-_{aq}}[A^-]_{aq,0} + C_5 \quad (55)$$

DOI: 10.1021/acs.molpharmaceut.5b00862
Mol. Pharmaceutics 2016, 13, 1030−1046

$$D_{HA_{aq}}\left(\frac{D_{R_{eff}}}{D_{HA_{eff}}}\right)^{2/3}\frac{\sqrt{K_{sp}(1+K_s^R[m])\left(1+\frac{K_a}{H_0^+}+K_s^{HA}[m]\right)}}{1+\frac{K_a}{H_0^+}+K_s^{HA}[m]} = D_{OH^-}[OH^-]_0 - D_{H^+}[H^+]_0 - D_{HA_m}[HA]_{m,0} + C_6 \quad (56)$$

and at $x = h$, since sink conditions are assumed, eqs 50-51 can be written as

$$C_2 h + C_5 = 0 \quad (57)$$

$$0 = D_{OH^-}[OH^-]_h - D_{H^+}[H^+]_h + C_3 h + C_6 \quad (58)$$

Combining eqs 55 to 58 and algebraically solving for interfacial pH, $[H^+]_0$, yields the following equation:

$$A[H^+]_0^{\,5} + B[H^+]_0^{\,4} + C[H^+]_0^{\,3} + D[H^+]_0^{\,2} + E[H^+]_0 + F = 0 \quad (59)$$

where

$$A = D_{H^+}^2(1+K_s^{HA}[m])$$

$$B = -2D_{H^+}(D_{H^+}[H^+]_h - D_{OH^-}[OH^-]_h)(1+K_s^{HA}[m]) + D_{H^+}^2 K_a$$

$$C = -2D_{H^+}D_{OH^-}K_w(1+K_s^{HA}[m]) + (1+K_s^{HA}[m])(D_{H^+}[H^+]_h - D_{OH^-}[OH^-]_h)^2 - 2D_{H^+}(D_{H^+}[H^+]_h - D_{OH^-}[OH^-]_h)K_a$$

$$D = 2D_{OH^-}K_w(D_{H^+}[H^+]_h - D_{OH^-}[OH^-]_h)(1+K_s^{HA}[m]) - 2D_{H^+}D_{OH^-}K_wK_a + (D_{H^+}[H^+]_h - D_{OH^-}[OH^-]_h)^2 K_a$$

$$E = (D_{OH^-}K_w)^2(1+K_s^{HA}[m]) + 2D_{OH^-}K_w(D_{H^+}[H^+]_h - D_{OH^-}[OH^-]_h)K_a - (D_{A^-_{aq}}^{1/3}D_{R_{eff}}^{2/3}K_a\sqrt{K_{sp}(1+K_s^R[m])})^2$$

$$F = K_a(D_{OH^-}K_w)^2$$

Evaluation of Flux of the Cocrystal Components

Applying the boundary conditions to eq 49, at $x = 0$:

$$D_{R_{aq}}\frac{\sqrt{K_{sp}(1+K_s^R[m])\left(1+\frac{K_a}{H_0^+}+K_s^{HA}[m]\right)}}{1+K_s^R[m]} = -D_{R_m}K_s^R[m]\frac{\sqrt{K_{sp}(1+K_s^R[m])\left(1+\frac{K_a}{H_0^+}+K_s^{HA}[m]\right)}}{1+K_s^R[m]} + C_4 \quad (60)$$

At $x = h$, assuming sink conditions:

$$0 = C_1 h + C_4 \quad (61)$$

Combining the above equations and solving for $-C_1$ for the flux of the cocrystal in terms of drug:

$$J_R = \frac{D_{R_{eff}}}{h_R}\sqrt{K_{sp}(1+K_s^R[m])\left(1+\frac{K_a}{H_0^+}+K_s^{HA}[m]\right)} \quad (62)$$

By substituting eq 10 into eq 62, it becomes

$$J_R = 0.62D_{R_{eff}}^{2/3}\omega^{1/2}\nu^{-1/6}\sqrt{K_{sp}(1+K_s^R[m])\left(1+\frac{K_a}{H_0^+}+K_s^{HA}[m]\right)} \quad (63)$$

The flux of the cocrystal in terms of coformer can be also solved in a similar manner by applying the boundary conditions to eq 50:

$$J_{HA} = \frac{D_{HA_{eff}}^{1/3}D_{R_{eff}}^{2/3}}{h_{HA}}\sqrt{K_{sp}(1+K_s^R[m])\left(1+\frac{K_a}{H_0^+}+K_s^{HA}[m]\right)} \quad (64)$$

By substituting eq 10 into eq 64, it can be shown to equal eq 63. This is expected since the flux of drug and coformer should be the same for a 1:1 cocrystal even though they have different diffusivities.

Interfacial Equilibrium Model

Given eqs 16, 27, 28, 29, and 53 and applying the equation for diffusion layer thickness shown in eq 10, the aqueous concentrations of R and HA at the dissolving surface required to maintain constant K_{sp} at all times $t \geq 0$ are as follows:

$$[R]_{aq,0} = \left(\frac{D_{HA_{eff}}}{D_{R_{eff}}}\right)^{1/3}\frac{\sqrt{K_{sp}(1+K_s^R[m])\left(1+\frac{K_a}{H_0^+}+K_s^{HA}[m]\right)}}{1+K_s^R[m]} \quad (65)$$

$$[HA]_{aq,0} = \left(\frac{D_{R_{eff}}}{D_{HA_{eff}}}\right)^{1/3}\frac{\sqrt{K_{sp}(1+K_s^R[m])\left(1+\frac{K_a}{H_0^+}+K_s^{HA}[m]\right)}}{1+\frac{K_a}{H_0^+}+K_s^{HA}[m]} \quad (66)$$

Based on eqs 65 and 66, the following boundary conditions for each species can be written for the interfacial equilibrium model At $x = 0$:

$$[R]_{aq,0} = \left(\frac{D_{HA_{eff}}}{D_{R_{eff}}}\right)^{1/3}\frac{\sqrt{K_{sp}(1+K_s^R[m])\left(1+\frac{K_a}{H_0^+}+K_s^{HA}[m]\right)}}{1+K_s^R[m]}$$

DOI: 10.1021/acs.molpharmaceut.5b00862
Mol. Pharmaceutics 2016, 13, 1030−1046

$$[\mathrm{HA}]_{\mathrm{aq},0} = \left(\frac{D_{\mathrm{R}_{\mathrm{eff}}}}{D_{\mathrm{HA}_{\mathrm{eff}}}}\right)^{1/3} \frac{\sqrt{K_{\mathrm{sp}}(1 + K_{\mathrm{s}}^{\mathrm{R}}[\mathrm{m}])\left(1 + \frac{K_{\mathrm{a}}}{[\mathrm{H}^+]_0} + K_{\mathrm{s}}^{\mathrm{HA}}[\mathrm{m}]\right)}}{1 + \frac{K_{\mathrm{a}}}{[\mathrm{H}^+]_0} + K_{\mathrm{s}}^{\mathrm{HA}}[\mathrm{m}]}$$

$$[\mathrm{R}]_{\mathrm{m},0} = \text{unknown}$$

$$[\mathrm{HA}]_{\mathrm{m},0} = \text{unknown}$$

$$[\mathrm{A}^-]_{\mathrm{aq},0} = \text{unknown}$$

$$[\mathrm{H}^+] = [\mathrm{H}^+]_0$$

$$[\mathrm{OH}^-] = [\mathrm{OH}^-]_0$$

At $x = h$:

$$[\mathrm{R}]_{\mathrm{aq},h} = 0 \text{ (under sink condition)}$$

$$[\mathrm{HA}]_{\mathrm{aq},h} = 0 \text{ (under sink condition)}$$

$$[\mathrm{R}]_{\mathrm{m},h} = 0 \text{ (under sink condition)}$$

$$[\mathrm{HA}]_{\mathrm{m},h} = 0 \text{ (under sink condition)}$$

$$[\mathrm{A}^-]_{\mathrm{aq},h} = 0 \text{ (under sink condition)}$$

$$[\mathrm{H}^+] = [\mathrm{H}^+]_h$$

$$[\mathrm{OH}^-] = [\mathrm{OH}^-]_h$$

Evaluation of pH at the Solid Surface

Applying the above boundary conditions to eqs 50 and 51, at $x = 0$:

$$D_{\mathrm{HA}_{\mathrm{aq}}}\left(\frac{D_{\mathrm{R}_{\mathrm{eff}}}}{D_{\mathrm{HA}_{\mathrm{eff}}}}\right)^{1/3} \frac{\sqrt{K_{\mathrm{sp}}(1 + K_{\mathrm{s}}^{\mathrm{R}}[\mathrm{m}])\left(1 + \frac{K_{\mathrm{a}}}{[\mathrm{H}^+]_0} + K_{\mathrm{s}}^{\mathrm{HA}}[\mathrm{m}]\right)}}{1 + \frac{K_{\mathrm{a}}}{[\mathrm{H}^+]_0} + K_{\mathrm{s}}^{\mathrm{HA}}[\mathrm{m}]} = -D_{\mathrm{HA}_{\mathrm{m}}}[\mathrm{HA}]_{\mathrm{m},0} - D_{\mathrm{A}_{\mathrm{aq}}^-}[\mathrm{A}^-]_{\mathrm{aq},0} + C_5 \quad (67)$$

$$D_{\mathrm{HA}_{\mathrm{aq}}}\left(\frac{D_{\mathrm{R}_{\mathrm{eff}}}}{D_{\mathrm{HA}_{\mathrm{eff}}}}\right)^{1/3} \frac{\sqrt{K_{\mathrm{sp}}(1 + K_{\mathrm{s}}^{\mathrm{R}}[\mathrm{m}])\left(1 + \frac{K_{\mathrm{a}}}{[\mathrm{H}^+]_0} + K_{\mathrm{s}}^{\mathrm{HA}}[\mathrm{m}]\right)}}{1 + \frac{K_{\mathrm{a}}}{[\mathrm{H}^+]_0} + K_{\mathrm{s}}^{\mathrm{HA}}[\mathrm{m}]} = D_{\mathrm{OH}^-}[\mathrm{OH}^-]_0 - D_{\mathrm{H}^+}[\mathrm{H}^+]_0 - D_{\mathrm{HA}_{\mathrm{m}}}[\mathrm{HA}]_{\mathrm{m},0} + C_6 \quad (68)$$

At $x = h$:

$$C_2 h + C_5 = 0 \quad (69)$$

$$0 = D_{\mathrm{OH}^-}[\mathrm{OH}^-]_h - D_{\mathrm{H}^+}[\mathrm{H}^+]_h + C_3 h + C_6 \quad (70)$$

Combining eqs 67 to 70 and algebraically solving for interfacial pH yields the following equation:

$$A[\mathrm{H}^+]_0^{\,5} + B[\mathrm{H}^+]_0^{\,4} + C[\mathrm{H}^+]_0^{\,3} + D[\mathrm{H}^+]_0^{\,2} + E[\mathrm{H}^+]_0 + F = 0 \quad (71)$$

where

$$A = D_{\mathrm{H}^+}^2(1 + K_{\mathrm{s}}^{\mathrm{HA}}[\mathrm{m}])$$

$$B = -2D_{\mathrm{H}^+}(D_{\mathrm{H}^+}[\mathrm{H}^+]_h - D_{\mathrm{OH}^-}[\mathrm{OH}^-]_h)(1 + K_{\mathrm{s}}^{\mathrm{HA}}[\mathrm{m}]) + D_{\mathrm{H}^+}^2 K_{\mathrm{a}}$$

$$C = -2D_{\mathrm{H}^+}D_{\mathrm{OH}^-}K_{\mathrm{w}}(1 + K_{\mathrm{s}}^{\mathrm{HA}}[\mathrm{m}]) + (1 + K_{\mathrm{s}}^{\mathrm{HA}}[\mathrm{m}])(D_{\mathrm{H}^+}[\mathrm{H}^+]_h - D_{\mathrm{OH}^-}[\mathrm{OH}^-]_h)^2 - 2D_{\mathrm{H}^+}(D_{\mathrm{H}^+}[\mathrm{H}^+]_h - D_{\mathrm{OH}^-}[\mathrm{OH}^-]_h)K_{\mathrm{a}}$$

$$D = 2D_{\mathrm{OH}^-}K_{\mathrm{w}}(D_{\mathrm{H}^+}[\mathrm{H}^+]_h - D_{\mathrm{OH}^-}[\mathrm{OH}^-]_h)(1 + K_{\mathrm{s}}^{\mathrm{HA}}[\mathrm{m}]) - 2D_{\mathrm{H}^+}D_{\mathrm{OH}^-}K_{\mathrm{w}}K_{\mathrm{a}} + (D_{\mathrm{H}^+}[\mathrm{H}^+]_h - D_{\mathrm{OH}^-}[\mathrm{OH}^-]_h)^2 K_{\mathrm{a}}$$

$$E = (D_{\mathrm{OH}^-}K_{\mathrm{w}})^2(1 + K_{\mathrm{s}}^{\mathrm{HA}}[\mathrm{m}]) + 2D_{\mathrm{OH}^-}K_{\mathrm{w}}(D_{\mathrm{H}^+}[\mathrm{H}^+]_h - D_{\mathrm{OH}^-}[\mathrm{OH}^-]_h)K_{\mathrm{a}} - (D_{\mathrm{A}_{\mathrm{aq}}^-}^{2/3}D_{\mathrm{R}_{\mathrm{eff}}}^{1/3}K_{\mathrm{a}}\sqrt{K_{\mathrm{sp}}(1 + K_{\mathrm{s}}^{\mathrm{R}}[\mathrm{m}])})^2$$

$$F = K_{\mathrm{a}}(D_{OH^-}K_{\mathrm{w}})^2$$

This equation is very similar to the one obtained from the surface saturation model. The only difference is the coefficient E in the equation because of the different boundary layer conditions.

Evaluation of Flux of the Cocrystal Components

Applying the new boundary conditions to mass balance eqs 49 and 50, the flux of the cocrystal in terms of components can be re-evaluated as

$$J_{\mathrm{R}} = J_{\mathrm{HA}} = 0.62(D_{\mathrm{R}_{\mathrm{eff}}}D_{\mathrm{HA}_{\mathrm{eff}}})^{1/3}\omega^{1/2}\nu^{-1/6}\sqrt{K_{\mathrm{sp}}(1 + K_{\mathrm{s}}^{\mathrm{R}}[\mathrm{m}])\left(1 + \frac{K_{\mathrm{a}}}{[\mathrm{H}^+]_0} + K_{\mathrm{s}}^{\mathrm{HA}}[\mathrm{m}]\right)} \quad (72)$$

Unlike the surface saturation model, the flux of the cocrystal is dependent on the effective diffusivity of not only the drug but also the coformer.

AUTHOR INFORMATION

Corresponding Author

*E-mail: geamidon@med.umich.edu.

Notes

The authors declare no competing financial interest.

ACKNOWLEDGMENTS

Research reported in this publication was partially supported by the National Institute of General Medical Sciences of the National Institutes of Health under Award No. R01GM107146. The content is solely the responsibility of the authors and does not necessarily represent the official views of the National

DOI: 10.1021/acs.molpharmaceut.5b00862
Mol. Pharmaceutics 2016, 13, 1030−1046

Institutes of Health. We also gratefully acknowledge partial financial support from the College of Pharmacy, University of Michigan.

REFERENCES

(1) Williams, H. D.; Trevaskis, N. L.; Charman, S. A.; Shanker, R. M.; Charman, W. N.; Pouton, C. W.; Porter, C. J. H. Strategies to Address Low Drug Solubility in Discovery and Development. *Pharmacol. Rev.* **2013**, *65*, 315−499.

(2) Schultheiss, N.; Newman, A. Pharmaceutical Cocrystals and Their Physicochemical Properties. *Cryst. Growth Des.* **2009**, *9* (6), 2950−2967.

(3) Thakuria, R.; Delori, A.; Jones, W.; Lipert, M. P.; Roy, L.; Rodriguez-Hornedo, N. Pharmaceutical Cocrystals and Poorly Soluble Drugs. *Int. J. Pharm.* **2013**, *453* (1), 101−125.

(4) Yadav, A. V.; Shete, A. S.; Dabke, A. P.; Kulkarni, P. V.; Sakhare, S. S. Co-Crystals: A Novel Approach to Modify Physicochemical Properties of Active Pharmaceutical Ingredients. *Indian Journal of Pharmaceutical Sciences* **2009**, *71* (4), 359−370.

(5) Weyna, D. R.; Cheney, M. L.; Shan, N.; Hanna, M.; Zaworotko, M. J.; Sava, V.; Song, S.; Sanchez-Ramos, J. R. Improving Solubility and Pharmacokinetics of Meloxicam via Multiple-Component Crystal Formation. *Mol. Pharmaceutics* **2012**, *9*, 2094−2102.

(6) Jung, M.; Kim, J.; Kim, M.; Alhalaweh, A.; Cho, W.; Hwang, S.; Velaga, S. P. Bioavailability of Indomethacin-Saccharin Cocrystals. *J. Pharm. Pharmacol.* **2010**, *62*, 1560−1568.

(7) Smith, A. J.; Kavuru, P.; Wojtas, L.; Zaworotko, M. J.; Shytle, R. D. Cocrystals of Quercetin with Improved Solubility and Oral Bioavailability. *Mol. Pharmaceutics* **2011**, *8* (5), 1867−1876.

(8) McNamara, D. P.; Childs, S. L.; Giordano, J.; Iarriccio, A.; Cassidy, J.; Shet, M. S.; Mannion, R.; O'Donnell, E.; Park, A. Use of a glutaric acid cocrystal to improve oral bioavailability of a low solubility API. *Pharm. Res.* **2006**, *23* (8), 1888−1897.

(9) Cheney, M. L.; Shan, N.; Healey, E. R.; Hanna, M.; Wojtas, L.; Zaworotko, M. J.; Sava, V.; Song, S.; Sanchez-Ramos, J. R. Effects of Crystal Form on Solubility and Pharmacokinetics: A Crystal Enginneering Case Study of Lamotrigine. *Cryst. Growth Des.* **2010**, *10*, 394−405.

(10) Shayanfar, A.; Jouyban, A. Physicochemical Characterization of a New Cocrystal of Ketoconazole. *Powder Technol.* **2014**, *262*, 242−248.

(11) Keramatnia, F.; Shayanfar, A.; Jouyban, A. Thermodynamic Solubility Profile of Carbamazepine-Cinnamic Acid Cocrystal at Different pH. *J. Pharm. Sci.* **2015**, *104* (8), 2559−65.

(12) Li, M.; Qiao, N.; Wang, K. Influence of Sodium Lauryl Sulfate and Tween 80 on Carbamazepine-Nicotinamide Cocrystal Solubility and Dissoluiton Behaviour. *Pharmaceutics* **2013**, *5* (4), 508−524.

(13) Alhalaweh, A.; Roy, L.; Rodriguez-Hornedo, N.; Velaga, S. P. pH-Dependent Solubility of Indomethacin-Saccharin and Carbamazepine-Saccharin Cocrystals in Aqueous Media. *Mol. Pharmaceutics* **2012**, *9*, 2605−2612.

(14) Bethune, S. J.; Huang, N.; Jayasankar, A.; Rodriguez-Hornedo, N. Understanding and Predicting the Effect of Cocrystal Components and pH on Cocrystal Solubility. *Cryst. Growth Des.* **2009**, *9* (9), 3976−3988.

(15) Roy, L. *Engineering Cocrystal and Cocrystalline Salt Solubility by Modulation of Solution Phase Chemistry*; Doctoral Dissertation; University of Michigan: 2013.

(16) Roy, L.; Lipert, M. P.; Rodriguez-Hornedo, N. Co-crystal Solubility and Thermodynamic Stability. *RSC Drug Discovery* **2012**, 247−279.

(17) Huang, N.; Rodriguez-Hornedo, N. Engineering Cocrystal Solubility, Stability, and pHmax by Micellar Solubilization. *J. Pharm. Sci.* **2011**, *100* (12), 5219−5234.

(18) Lee, H. G.; Zhang, G. G. Z.; Flanagan, D. R. Cocrystal Intrinsic Dissolution Behavior Using a Rotating Disk. *J. Pharm. Sci.* **2011**, *100* (5), 1736−1744.

(19) Qiao, N.; Wang, K.; Schlindwein, W.; Davies, A.; Li, M. In Situ Monitoring of Carbamazepine-Nicotinamide Cocrystal Intrinsic Dissolution Behaviour. *Eur. J. Pharm. Biopharm.* **2013**, *83* (3), 415−426.

(20) Childs, S. L.; Chyall, L. J.; Dunlap, J. T.; Smolenskaya, V. N.; Stahly, B. C.; Stahly, G. P. Crystal Engineering Approach to Forming Cocrystals of Amine Hydrochlorides with Organic Acids. Molecular Complexes of Fluoxetine Hydrochloride with Benzoic, Succinic, and Fumaric Aicds. *J. Am. Chem. Soc.* **2004**, *126*, 13335−13342.

(21) Shiraki, K.; Takata, N.; Takano, R.; Hayashi, Y.; Terada, K. Dissolution Improvement and the Mechanism of the Improvement from Cocrystallization of Poorly Water-soluble Compounds. *Pharm. Res.* **2008**, *25* (11), 2581−2592.

(22) Huang, N.; Rodriguez-Hornedo, N. Effect of Micellar Solubilization on Cocrystal Solubility and Stability. *Cryst. Growth Des.* **2010**, *10*, 2050−2053.

(23) Huang, N.; Rodriguez-Hornedo, N. Engineering Cocrystal Thermodynamic Stability and Eutectic Points by Micellar Solubilization and Ionization. *CrystEngComm* **2011**, *13*, 5409−5422.

(24) Mooney, K. G.; Mintun, M. A.; Himmelstein, K. J.; Stella, V. J. Dissolution Kinetics of Carboxylic Acids I: Effect of pH under Unbuffered Conditions. *J. Pharm. Sci.* **1981**, *70* (1), 13−22.

(25) Higuchi, W. I.; Mir, N. A.; Desai, S. J. Dissolution Rates of Polyphase Mixtures. *J. Pharm. Sci.* **1965**, *54* (10), 1405−1410.

(26) Rodriguez-Hornedo, N.; Nehm, S. J.; Seefeldt, K. F.; Pagan-Torres, Y.; Falkiewicz, C. J. Reaction Crystallization of Pharmaceutical Molecular Complexes. *Mol. Pharmaceutics* **2006**, *3* (3), 362−367.

(27) Good, D. J.; Rodriguez-Hornedo, N. Solubility Advantage of pHarmaceutical Cocrystals. *Cryst. Growth Des.* **2009**, *9* (5), 2252−2264.

(28) Nernst, W. Theorie der Reaktionsgeschwindigkeit in heterogenen systemen. *Zeitschrift für Physikalische Chemie* **1904**, *47*, 52−55.

(29) Kabir-ud-Din; David, S. L.; Kumar, S. Viscosities of Sodium Dodecyl Sulfate Solutions in Aqueous Ammonium Salts. *J. Chem. Eng. Data* **1997**, *42* (6), 1224−1226.

(30) Poskanzer, A. M.; Goodrich, F. C. Surface Viscosity of Sodium Dodecyl Sulfate Solutions with and without Added Dodecanol. *J. Phys. Chem.* **1975**, *79* (20), 2122−2126.

(31) Brunner, E. Reaktionsgeschwindigkeit in Heterogenen Systemen. *Zeitschrift für Physikalische Chemie* **1904**, *47*, 56−102.

(32) Levich, V. G. *Physico-chemical Hydrodynamics*. Prentice-Hall: Englewood Cliffs, N.J., 1962.

(33) Othmer, D. F.; Thakar, M. S. Correlating Diffusion Coefficients in Liquids. *Ind. Eng. Chem.* **1953**, *45* (3), 589−593.

(34) Rangel-Yagui, C. O.; Junior Pessoa, A.; Tavares, L. C. Micellar Solubilization of Drugs. *J. Pharm. Sci.* **2005**, *8* (2), 147−163.

(35) Imae, T.; Abe, A.; Taguchi, Y.; Ikeda, S. Solubilization of a Water-Insoluble Dye in Aqueous Solutions of Dodecyltrimethylammonium Halides, and Its Relation to Micelle Size and Shape. *J. Colloid Interface Sci.* **1986**, *109* (2), 567−575.

(36) Birdi, K. S. *Handbook of Surface and Colloid Chemistry*, 3rd ed.; CRC Press: 2008.

(37) Amidon, G. E.; Higuchi, W. I.; Ho, N. F. H. Theoretical and Experimental Studies of Transport of Micelle-Solubilized Solutes. *J. Pharm. Sci.* **1982**, *71* (1), 77−84.

(38) Rao, V. M.; Lin, M.; Larive, C. K.; Southard, M. Z. A Mechanistic Study of Griseofulvin Dissolution into Surfactant Solutions Under Laminar Flow Conditions. *J. Pharm. Sci.* **1997**, *86* (10), 1132−1137.

(39) Sun, W.; Larive, C. K.; Southard, M. Z. A Mechanistic Study of Danazol Dissolution in Ionic Surfactant Solutions. *J. Pharm. Sci.* **2003**, *92* (2), 424−435.

(40) Chen, A.; Wu, D.; Johnson, C. S. Determination of the Binding Isotherm and Size of the Bovine Serum Albumin-Sodium Dodecyl Sulfate Coomplex by Diffusion-Ordered 2D NMR. *J. Phys. Chem.* **1995**, *99* (2), 828−834.

(41) Cussler, E. L. *Diffusion Mass Transfer in Fluid Systems*, 2nd ed.; Cambridge University Press: New York, 1997.

DOI: 10.1021/acs.molpharmaceut.5b00862
Mol. Pharmaceutics 2016, 13, 1030−1046